ELSEVIER

Chemical Geology 167 (2000) 25–51

CHEMICAL GEOLOGY
INCLUDING
ISOTOPE GEOSCIENCE

www.elsevier.com/locate/chemgeo

Reaction pathways in the Fe–S system below 100°C

Liane G. Benning *, Rick T. Wilkin [1], H.L. Barnes

Department of Geosciences, Pennsylvania State University, University Park, PA 16802, USA

Received 18 November 1998; received in revised form 13 April 1999

Abstract

The formation pathways of pyrite are controversial. Time resolved experiments show that in reduced sulphur solutions at low temperature, the iron monosulphide mackinawite is stable for up to 4 months. Below 100°C, the rate of pyrite formation from a precursor mackinawite is insignificant in solutions equilibrated solely with $H_2S_{(aq)}$. Mackinawite serves as a precursor to pyrite formation only in more oxidised solutions. Controlled, intentional oxidation experiments below 100°C and over a wide range of pH (3.3–12) confirm that the mackinawite to pyrite transformation occurs in slightly oxidising environments. The conversion to pyrite is a multi-step reaction process involving changes in aqueous sulphur species causing solid state transformation of mackinawite to pyrite via the intermediate monosulphide greigite. Oxidised surfaces of precursors or of pyrite seeds speed up the transformation reaction.

Solution compositions from the ageing experiments were used to derive stability constants for mackinawite from 25°C to 95°C for the reaction:

$$FeS(s) + 2H^+ \Leftrightarrow Fe^{2+} + H_2S$$

The values of the equilibrium constant, $\log K_{FeS}$, varied from 3.1 at 25°C to 1.2 at 95°C and fit a linear, temperature-dependent equation: $\log K_{FeS} = 2848.779/T - 6.347$, with T in Kelvin. From these constants, the thermodynamic functions were derived. These are the first high temperature data for the solubility of mackinawite, where Fe^{2+} is the dominant aqueous ferrous species in reduced, weakly acidic to acidic solutions.

Keywords: Iron sulphides; Mackinawite; Greigite; Pyrite; Reaction pathways; Solubility

1. Introduction

Pyrite is the most common ore mineral but the factors that control its formation are still equivocal. The roles of authigenic iron sulphides in regulating and controlling the global geochemical iron and sulphur cycles, as well as the wide range of industrial applications for pyrite (i.e., semiconductors, high energy batteries, solar cells), have led to much research on its physical and chemical properties and mechanisms of formation. At temperatures above 350°C, the Fe–S system has been extensively studied and phase relations are well known (see Vaughan and Craig, 1997 for a review). However, largely neglected are the hydrothermal processes of pyrite

* Corresponding author. School of Earth Sciences, University of Leeds, Leeds LS2 9JT, UK. Tel.: +44-113-233-5220; fax: +44-113-233-5259.

E-mail address: liane@earth.leeds.ac.uk (L.G. Benning).

[1] Present address: US Environmental Protection Agency, National Risk Management Research Laboratory, Ada, OK 74820, USA.

0009-2541/00/$ - see front matter
PII: S0009-2541(99)00198-9

nucleation and growth. At low temperatures, the mechanisms and pathways of pyrite formation in aqueous solutions are far better studied, but the dominant reaction pathways remain controversial and their rates are known only generally.

The importance of an iron monosulphide precursor to pyrite formation has been recognised since the early work of Allen et al. (1912). Mackinawite (Fe_9S_8), has a chemical composition varying from $Fe_{0.87}S$ to $FeS_{1.1}$ (Berner, 1964; Rickard, 1969,1975; Sweeney and Kaplan, 1973), however, in this study mackinawite will nominally be written as FeS. Field observations of anoxic sediments indicate the presence and persistence of precursor iron monosulphides (AVS, acid-volatile sulphides: mackinawite and greigite) and their involvement in pyrite formation processes (e.g., Berner, 1970; Jørgensen, 1977; Boesen and Postma, 1988; Canfield et al., 1992; Krupp, 1994; Wilkin and Barnes, 1997; Lyons, 1997; Hurtgen et al., 1999). In the last 70 to 85 years, many experiments have shown that an oxidant is required to produce pyrite from precursor iron monosulphides. It is generally accepted that aqueous sulphur species with oxidation states intermediate between sulphate and sulphide are important to pyrite formation processes (e.g., Berner, 1967, 1970; Rickard, 1969, 1975; Roberts et al., 1969; Taylor et al., 1979a,b; Luther, 1991; Schoonen and Barnes, 1991b; Wilkin and Barnes, 1996; Benning and Barnes, 1998). Taylor et al. (1979a) and Wilkin and Barnes (1996) discussed the role of oxygen in producing these sulphur intermediates and its involvement as a direct reactant in pyrite formation. In addition, it is generally accepted that the low temperature conversion of mackinawite to pyrite proceeds via the mixed Fe^{2+}/Fe^{3+} valence phase greigite, Fe_3S_4.

An important corollary of the above studies is that the dominant formation path of pyrite is by reactions between a precursor monosulphide and zero-valent sulphur species (Polysulphide 'pathway'). The reaction mechanism for this pathway has often been assumed to follow sulphidation of an iron monosulphide (assuming FeS stoichiometry):

$$FeS(s) + S^{\circ}(s) \rightarrow FeS_2(s) \quad (1)$$

or

$$FeS(s) + S_n^{2-} \rightarrow FeS_2(s) + S_{n-1}^{2-} \quad (1a)$$

Recent experiments, however, using sulphur isotope ratios as reaction tracers indicate that iron disulphide nucleation proceeds via loss of ferrous iron from the precursor monosulphide rather than via addition of zero-valent sulphur (Wilkin and Barnes, 1996):

$$2FeS(s) + 2H^+ \rightarrow FeS_2(s) + Fe^{2+} + H_2(g) \quad (2)$$

These results confirmed the interpretation of calculated molar volume changes accompanying pyrite formation by iron-loss and sulphur-addition pathways (Furukawa and Barnes, 1995). In addition, in-situ X-ray powder diffraction studies indicate that the mackinawite to greigite transformation follows a coupled oxidation and iron-loss mechanism (Lennie et al., 1997).

Recently, however, an alternative pathway has been proposed by Wächtershäuser (1988, 1993) who suggested that besides zero-valent sulphur species, H_2S could also oxidise monosulphides and form pyrite via the 'H_2S-pathway':

$$FeS(s) + H_2S \rightarrow FeS_2(s) + H_2(g) \quad (3)$$

This reaction suggested to have important implications on the origin of primordial metabolic cycles because pyrite surfaces could act as ideal catalytic sites and the produced hydrogen would be an energy source for bacterial life. Wächtershäuser (1988, 1993) suggested that the conversion of FeS to FeS_2 could be coupled to the reduction of CO or CO_2 forming simple organic molecules. However, conclusive evidence substantiating these hypotheses is still lacking. Experiments and theoretical calculations conducted by Drobner et al. (1990), and more recently by Rickard (1997) and Rickard and Luther (1997), have shown that pyrite formation via the reaction between a monosulphide precursor with H_2S is a very fast process at temperatures below 125°C. These observations, however, are inconsistent with results obtained from numerous studies conducted in various independent laboratories (Berner, 1964, 1970; Rickard, 1969, 1975; Roberts et al., 1969; Taylor et al. 1979a; Schoonen and Barnes, 1991a,b,c; Wilkin and Barnes, 1996 and references therein). These studies have demonstrated that pyrite formation proceeds at significant rates only with an oxidant other than H_2S.

This paper presents new experimental data on the stability of mackinawite and the conversion of iron monosulphide to pyrite via various oxidative steps. It is shown that as long as the iron monosulphide is kept in a reducing atmosphere, devoid of any reactant other than H_2S, mackinawite is the stable phase and the formation of pyrite is inhibited over a wide range of pH and temperature. Only oxidation, either of the aqueous sulphur species or of the precursor mackinawite, induces pyrite formation.

2. Methods and materials

2.1. Experimental method

In-situ precipitation, ageing and conversion experiments were conducted in sealed 500 ml, glass reaction vessels with covers having four ground glass ports. The ports were fitted with (1) a condenser/thermometer junction, (2) an injection and sampling assembly, (3) an H_2S gas inlet and outlet, and (4) a lyophiliser attachment and N_2-gas inlet port (Fig. 1). The temperature of the system was adjusted between 25°C and 95°C ($\pm$0.5°C) by using a heating mantle around the glass reaction vessel. The gas inlet port fulfilled a dual purpose; by keeping a constant flow of reduced gas through the solutions, mixing and reducing conditions were ensured (Murowchick and Barnes, 1986; Wilkin and Barnes, 1996). All inorganic salts and gases, unless otherwise specified, were reagent grade.

Throughout all experiments, special care was taken to avoid oxygen contamination (except where oxidation was deliberate). Ultra high-purity grade nitrogen gas was additionally purified via a double oxygen scrubber unit (Alltech®). The resulting oxygen-free nitrogen (OFN_2) was used in all experiments. A weighed quantity of Mohr's salt (ferrous ammonium sulphate hexahydrate — $Fe(NH_4)_2(SO_4)_2 \cdot 6H_2O$, Aldrich®) was transferred to a reaction vessel which was evacuated and re-equilibrated with OFN_2 for $\sim$30 min. To produce a low pH, O_2-free solution of known Fe^{2+} concentration (0.115–0.023 *m*, $3.2 < pH < 3.9$) double distilled water was freshly boiled and cooled under a constant flow of OFN_2 and then transferred under a positive OFN_2 pressure into the reaction vessel. Subsequently, the system was heated to the desired temperature, and the solution and the gas headspace were saturated with pure H_2S gas (C.P. grade, 99.5% H_2S, MG Industries). Before entering the reaction vessel, in order to water-saturate the input gas, the

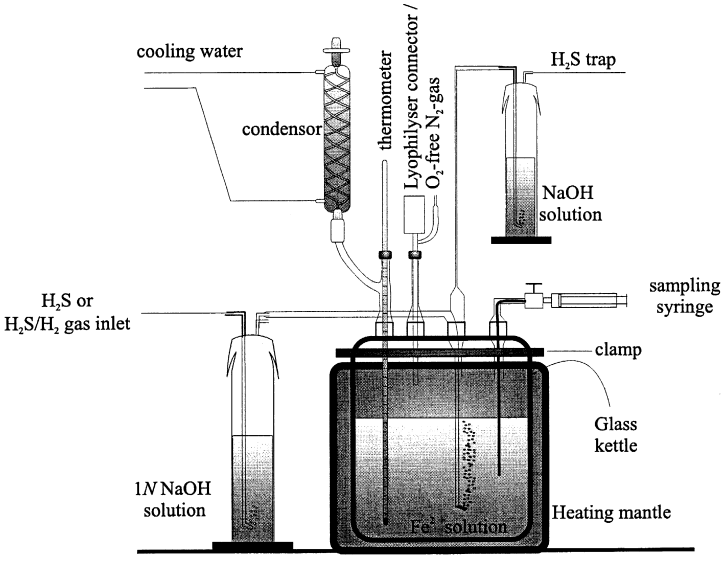

Fig. 1. Experimental set-up for the in situ precipitation and ageing experiments.

H_2S was passed at 1 bar through a freshly prepared oxygen-free 1 N NaOH solution. Following this step, a H_2S-saturated Fe^{2+} solution of acid pH (< 4) was obtained, yet, due to the high solubility of iron monosulphides under acid conditions only partial precipitation occurred (Berner, 1967, 1970; Rickard, 1975; Schoonen and Barnes, 1991a b c).

Precipitation of the bulk iron monosulphides was induced by injecting 5–100 ml of freshly prepared, oxygen free 1 N NaOH solution into the reaction vessel, while the positive H_2S gas overpressure was continuously maintained and mixing was ensured. In this way, the pH of the experimental solutions could be adjusted initially to values between 3.3 and 12. After 5–10 min, a sample of the jet-black slurry was extracted and immediately characterised (see below). In all experiments, after this step the only observed solid was mackinawite of different degrees of crystallinity. After another hour of equilibrating with H_2S gas, an additional sample was withdrawn and characterised. Subsequently, the overpressure-gas was switched to a H_2S/H_2 gas-mixture of different ratios (1%, 10%, 25%, 50% and 100% H_2S in H_2). These gases maintained a reduced atmosphere above the suspension and the oxidation state was controlled by the partial pressure of hydrogen in the gas mixture. Throughout the experiments (except in specified runs) the chosen gas mixture was steadily bubbled through the experimental solution, thus maintaining constant pH conditions, an uninterrupted oxygen-free environment, and continuous mixing. Assuming equilibrium conditions, a plot of the ratio between hydrogen fugacity and hydrogen sulphide activity, $\log(f_{H_2}/a_{H_2S})$, vs. temperature (Fig. 2), shows that all experiments carried out in this study were within the stability field of pyrite. Within this field, barring any kinetic restrictions the precursor mackinawite should readily react to form pyrite.

2.2. Solution and solid characterisation

At different time intervals (5 min to 4 months), samples of the suspension were withdrawn with a 20 ml syringe attached to a teflon sampling device (Fig. 1). After immediate transfer of the syringe to an OFN_2-filled glove bag, the samples were filtered through 0.2-μm polycarbonate filters (Corning®) and analysed as described below.

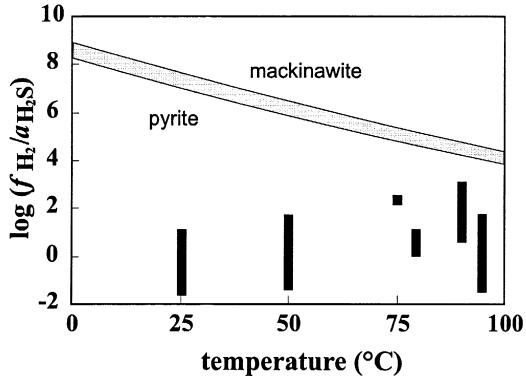

Fig. 2. Ratio between the hydrogen fugacity and the activity of aqueous H_2S, plotted as a function of temperature. The thermodynamic calculations indicate that, all experiments carried out in this study were supersaturated with respect to pyrite. Bars show the spread of experimental conditions at each temperature. The grey band indicates the uncertainty in the equilibrium conditions between pyrite and mackinawite. Data for mackinawite are from this study, for pyrite from Robie et al. (1978) and for H_2S from Wagman et al. (1968).

The pH of the filtered solutions was measured at 25°C using a sulphide-tolerant glass combination electrode (Corning®), calibrated against NIST-traceable buffer solutions. Total dissolved iron (ΣFe) and sodium (ΣNa) were determined using inductively coupled plasma spectroscopy (ICPS, Leeman PS3000) after fixing with 1 *m* HCl. In some experiments, dissolved Fe^{2+} was measured colorimetrically using the ferrozine method after Landing and Westerlund (1988), and this was used as a cross check with the total dissolved iron. Total reduced aqueous sulphur ($\Sigma S_{red(aq)}$) was measured with an S-coulometer after fixing the $\Sigma S_{red(aq)}$) as bisulphide with 1 N NaOH and reacting the alkaline solution with 6 M HCl releasing H_2S gas, which was quantitatively titrated (see below).

After filtration, the solids were immediately transferred under a nitrogen atmosphere into an oxygen-free N_2-filled desiccator and dried under vacuum. Within 10–30 min after extraction, the samples were characterised using X-ray diffraction (XRD, Rigaku Geigerflex, CuKα radiation, scanning rate 2°/min for a 2θ range of 5–65°) and scanning electron microscopy with an energy dispersive system (SEM-EDS, Phillips, XL-20). In addition, the magnetic state of the dried powders was checked with a hand

magnet. Caution is warranted here, because some samples when filtered and dried under carefully controlled oxygen-free conditions and subsequently exposed to air, started an intense exothermic reaction — they spontaneously self-ignited. The filtered material burns and a strong odour of SO_2 evolves. However, this self-ignition could not be used as an indicator of perfectly controlled, O_2-free conditions, because the self-ignition was irregular. The reaction products of a self-ignition process, determined immediately after the burning was completed, yielded X-ray peaks for greigite, goethite and pyrite. Parallel collected samples, without self-ignition gave a clear mackinawite X-ray pattern.

In order to quantify the conversion rates of iron monosulphides to pyrite, the relative amounts of ''FeS'' to FeS_2 were determined via a sequential extraction method using a sulphur coulometer (Atkin and Sommerfield, 1994; Canfield et al., 1986). At each sampling interval, ~3 ml of the suspension was filtered in a glove bag under oxygen-free N_2. The solid fraction was immediately reacted in a first step with 10 ml of 6 M HCl solution, which dissolved the iron monosulphide phases (AVS) producing H_2S. In a second step, the remaining solids (iron disulphides and elemental sulphur) were dissolved in 10 ml of $CrCl_2$-HCl solution also producing H_2S. Both steps were carried out for 15 min each while the solutions were heated and stirred. The resulting H_2S gas was flushed via N_2 gas to a coulometer (UIC, CM 3200) and quantitatively titrated. The relative amounts of gas produced in the two steps were used as a measure of reaction progress.

The precision of all measurements was tested by concurrently processing two to three samples. The analytical uncertainties were below 0.15 log units for the pH determinations, 3–5% for ΣFe, and ΣNa^+ measurements, and ~4–6% for the coulometric method.

2.3. Controlled, intentional oxidation experiments

In selected experiments, oxidation was used to test for changes in reaction speed and reaction mechanism of pyrite formation (SO-and FO-runs in Tables 1 and 2). Initially, the procedures described above for precipitation and ageing of the iron monosulphide precursors were followed, and the precipitated monosulphides were consequently aged for 4 days to 3.5 months. The solid product was found to be mackinawite. Subsequently, two procedures were tested: (1) ''Fast Oxidation'', FO-runs: instead of the reduced gas mixture, oxygen or air (i.e., 20% oxygen) was bubbled directly through the solutions (Wilkin and Barnes, 1996). (2) ''Slow Oxidation'', SO-runs: the reduced gas flow was stopped and in some cases one port of the kettle was opened to the atmosphere allowing slow oxidation to take place. The characterisation of the solutions and solids in these experiments followed the same steps as described above.

2.4. Freeze-dried precursor

To test the influence of surface oxidation and area of the monosulphide precursor on the reaction rate and also to reproduce previous experiments (Rickard, 1997), several runs were performed using freeze-dried precursor materials (FD-runs in Tables 1 and 2). Initially, ageing experiments conducted as described above yielded mackinawite as the only solid phase after 5–7 days. Subsequently, the flow of H_2S through the solutions (i.e., mixing) was stopped, and the gas in the headspace above the solution was replaced with continuously flowing oxygen-free N_2. Settling of the precipitate in an oxygen-free environment was thus ensured. After ~5–7 h under constant inert gas flow, the clear supernatant solution was withdrawn from above the black precipitate with a 60 ml syringe through a port of the reaction vessel. With the remaining slurry, two freeze-drying procedures were tested: (1) Ex situ freeze-drying (ES-FD): the slurry was collected into syringes and transferred into oxygen-free N_2-flushed, 50 ml bottles. These bottles were placed into a lyophiliser chamber (in air) and freeze-dried under vacuum (72 h). This ex situ freeze-drying procedure was performed as fast as possible in order to minimise oxidation. (2) In-situ freeze-drying (IS-FD) was carried out, by directly attaching the reaction vessel (Fig. 1) to an outer vacuum port of the lyophilising unit. The bottom slurry was then freeze-dried for 170 h. In both procedures much care was taken to avoid oxygen contamination, although partial oxidation cannot be ruled out, especially in the ex situ procedure. The

Table 1
Experimental conditions and products

Run #	Temp. (°C)	Time history	Flush gas	$pH_{25°C}$	ΣFe (ppm)	H_2S (m)	Wt.% 'FeS'	Wt.% $FeS_2 + S°$	Products in order of abundance as determined by XRD and coulometry[a]
RF	25	48	99.5% H_2S	4.45	2565[b]/31	0.007	100	0	mack
A1	50	0.5 h	99.5% H_2S	4.28	2456[b]/1.31	0.065	100	0	mack
		192 h	10% H_2S	4.51	1.20	0.043	96	< 4	mack
SO1	50	72 h	0% H_2S	4.94	n.d.	0.012	84	16	mack, gr, py, s, magnetic
A2	50	0.5 h	99.5% H_2S	4.86	2044[b]/2.51	0.0082	97	3	mack
		1944 h	99.5% H_2S	4.58	2.39	0.0075	95	5	mack
A3	95	168 h	50% H_2S	3.57	1300[b]/265	n.d.	95	< 5	mack
S1		+ cubes + 0.5 h	50% H_2S	3.66	260	n.d.	92	8	mack, py, not magnetic
		120 h	50% H_2S	3.68	252	n.d.	88	12	mack, py, not magnetic
SO2		216 h	0% H_2S	3.69	239	n.d.	40	60	py, mack, gr, s, magnetic
A4	50	120 h	10% H_2S	4.54	2350[b]/0.39	0.088	95	5	mack
SO3		120 h	0% H_2S	4.92	n.d.	0.029	90	10	mack ± gr, py, magnetic
FO1		+ 1 h air	0% H_2S	6.12	n.d.	0.006	49	51	py, mack, gr, s, goe, magnetic
		+ 0.5 h air	0% H_2S	6.3	n.d.	0.004	13	87	py, gr, magnetic
		+ 84 h	0% H_2S	6.5	n.d.	n.d.	3	97	py, ± s, magnetic
A5	50	2850 h	99.5% H_2S	4.6	n.d.	n.d.	100	0	mack
SO4		+ 336 h	0% H_2S	5.2	n.d.	n.d.	61	39	gr, mack, py, magnetic
A6	50	432 h	50% H_2S	3.9	n.d.	n.d.	98	2	mack
SO5		288 h	0% H_2S	5.5	n.d.	n.d.	37	63	py, gr, mack, magnetic
A7	80	24 h	99.5% H_2S	8.15	2230[b]/0.17	0.0068	98	2	mack
		528 h	0% H_2S	8.23	n.d.	0.0031	100	0	mack
SO6		264 h	0% H_2S	8.2	n.d.	0.0013	74	26	gr, mack, py, s, magnetic
		1664 h	0% H_2S	8.6	n.d.	n.d.	< 5	95[c]	py, hem, goe,
A8	80	147 h	50% H_2S	3.24	6400[b]/433	n.d.	100	< 5	mack
FO2		+ 0.58 h air + 5 h	0% H_2S	6.1	n.d.	n.d.	n.d.	n.d.	mack, gr, goe, ± py, ± s, magnetic
		3 h + 0.5 h air	0% H_2S	5.4	n.d.	n.d.	n.d.	n.d.	gr, mack, goe, s, py, magnetic
		+ 8 h + 1 h air	0% H_2S	4.5	n.d.	n.d.	n.d.	n.d.	gr, py, s, goe, mack, magnetic
		24 h	0% H_2S	3.6	n.d.	n.d.	n.d.	n.d.	py, goe, gr, magnetic
		185 h	0% H_2S	3.8	n.d.	n.d.	< 5	100[c]	py, ± goe, magnetic

A9	90	2 h	99.5% H_2S	3.86	2350[b]/66.96	0.0014	95	5	mack
SO7		468 h + air	10% H_2S	4.23	n.d.	0.0015	87	13	mack, ±py, magnetic
A10	75	136 h	1% H_2S	4.52	2130[b]/2.81	0.0044	98	2	mack
A11		216 h	1% H_2S	11.9	n.d.	0.0041	100	0	mack
SO8		2560 h	0% H_2S	11.9	n.d.	0.0040	100	0[c]	mack[d]
A12	80	96 h	50% H_2S	7.39	1260[b]/0.69	0.061	98	2	mack
SO9		70/75 h	0% H_2S	7.31	< 1	0.055	69	31	mack, gr, s, py, magnetic
		243 h	0% H_2S	7.91	< 1	0.035	39	61	gr, s, py, ±mack, magnetic
		579 h	0% H_2S	8.83	< 1	0.017	23	77	py, gr, magnetic
		939 h	0% H_2S	6.96	< 1	n.d.	4	96	py, magnetic
A13	90	132 h	50% H_2S	3.34	2240[b]/ < 1	n.d.	100	0	mack
SO10		48 h, open system	100% air	3.38	n.d.	n.d.	n.d.	n.d.	mack, gr, py, goe, s, magnetic
		154 h	100% air	n.d.	n.d.	n.d.	n.d.	n.d.	py, goe, gr, s, magnetic
		220 h	100% air	4.2	n.d.	n.d.	n.d.	n.d.	py, ±goe[e], ±s[e], magnetic
A14	25	416 h	50% H_2S	7.1	1560[b]/ < 10	n.d.	100	0	mack
SO11		258 h	0% H_2S	4.9	< 10	n.d.	n.d.	n.d.	mack, s, gr, py, magnetic
A15	95	173 h	50% H_2S	3.6	1355[b]/ < 10	0.0133	95	< 5	mack
SO12		24 h	0% H_2S	3.69	n.d.	0.0130	92	8	mack, gr, py, s, magnetic
		98 h	0% H_2S	n.d.	n.d.	0.0128	82	18	gr, mack, py, s, magnetic
		240 h	0% H_2S	n.d.	n.d.	0.0044	32	68	py, mack/gr, s, magnetic
A16	25	326 h	99.5% H_2S	4.5	2650[b]/2.76	0.08	95	< 5	mack
FO3	25	+ 2.5 h air + 24 h	100% air	6.9	n.d.	n.d.	0	100[c]	py, ±goe, s, magnetic
A17	25	5 h	99.5% H_2S	12.5	1250[b]/ < 1	n.d.	100[c]	0	mack
SO13	25	48 h	100% air	12.3	n.d.	n.d.	100[c]	0	mack[d]
IS-FD	25	72 h[f]	99.5% H_2S	4.3	2299[b]/n.d.	0.008	98	2	FD-mack
		42 h	100% H_2	4.1	n.d.	~ 0.1[g]	100	0	mack
		24 h	99.5% H_2S	n.d.	n.d.	~ 0.1	91	9	mack, s
		66 h	99.5% H_2S	4.95	n.d.	~ 0.1	36	64	py, mack, gr, magnetic
		218 h	99.5% H_2S	6.3	n.d.	~ 0.1	0	100	py, not magnetic
ES-FD1	25	24 h	25% H_2S	4.9	n.d.	~ 0.1	22	78	py, ±mack/gr, s, magnetic
ES-FD2	95	85 h	100% H_2S	3.8	n.d.	~ 0.1	< 5	> 95	py, s, ±mack/gr, magnetic

[a] Mack: mackinawite; gr: greigite; py: pyrite; goe: goethite; s: sulphur; hem: hematite.
[b] Initial Fe^{2+} concentration.
[c] Estimated from XRD patterns.
[d] Although SO experiments, no other phases formed; possibly alkaline pH increases stability?
[e] Not in XRD patterns but visible at solution, air-space interface.
[f] First line in the IS-FE experiment represents the ageing of the precursor material before freeze-drying.
[g] Fresh, oxygen-free H_2S saturated solution.

Table 2
Summary of experimental conditions and products

Run #	Temp. (°C)	Σ time (days)	pH_{final}	Final solids[a]	Run #	Σ time (days)	pH_{final}	Final solids[a]	Run #	Σ time (days)	pH_{final}	Final solids[a]
RF	25	2	4.5	m								
A14	25	17.3	7.1	m	SO11	10.8[b]	4.9	m,s,g,p				
A16	25	14.8	4.5	m					FO3	1.1[b]	6.9	p ± go
A17	25	0.21	12.5	m	SO13	2	12.3	m[c]				
A1	50	8	4.5	m	SO1	3[b]	4.9	m,g,p,s				
A2	50	81	4.6	m								
A4	50	5	4.5	m	SO3	5[b]	4.9	m, ± g,p	FO1	3.6[b]	6.5	p ± s
A5	50	118.8	4.6	m	SO4	14[b]	5.2	g,m,p				
A6	50	18	3.9	m	SO5	12[b]	5.5	p,g,m				
A10	75	5.7	4.5	m								
A11	75	9	11.9	m	SO8	106.7	11.9	m[c]				
A7	80	22	8.2	m	SO6	69.3	8.6	p,h,go				
A8	80	6	3.2	m					FO2	9.5[b]	3.8	p ± go
A12	80	4	7.4	m	SO9	39.1[b]	7.0	p				
A9	90	0.08	3.9	m	SO7	19.5[b]	4.2	m, ± p				
A13	90	5.5	3.3	m	SO10	9.2[b]	4.2	p				
A15	95	13.6	3.6	m	SO12	10[b]	–	p,m/g,s				
A3	95	6	3.6	m	SO2	9[b]	3.7	p,m,g,s				
S1	95	3.1	3.7	m,p								
IS-FD	25	13.8	6.3[d]	p,m/g,s								
ES-FD1	25	1	4.9[d]	p,m/g,s								
ES-FD2	95	3.5	3.8[d]	p,s,m/g								

[a] m: mackinawite; g: greigite; p: pyrite; s: sulphur; go: goethite; h: hematite.
[b] Magnetic.
[c] Although SO run, product only mackinawite; note high pH.
[d] pH of slurry measured after re-equilibration with new H_2S solution.

freeze-dried materials were characterised by XRD and SEM. In addition, the surface area of the ex situ freeze-dried mackinawite (procedure 1) was determined using N_2 and Kr-BET. The ex situ freeze-dried material was ground in acetone in a glove box under oxygen-free N_2 and anoxically transferred into the BET sample holders. Prior to surface area determination, the samples were evacuated for 84 h at 100°C.

Once the material was freeze-dried it was re-equilibrated with freshly prepared 0.1 *m* O_2-free H_2S solution (prepared as described above) and the reaction progress was observed over time and with varying degrees of reducing power (i.e., different gas saturation).

2.5. ''Seeding'' experiment

Pyrite seeds were added to a well-aged mackinawite slurry to test whether the oxidised surfaces of natural pyrite cubes provide a reactive surface for pyrite nucleation. The seeds were 0.6–1.5 mm pyrite cubes from Navajun, Spain (Calvo and Sevillano, 1989). The total surface area of the pyrite cubes was calculated to be ~ 70 mm^2, thus extremely small in comparison with the overall surface area of the mackinawite in the suspension, tens of m^2 (see freeze-dried section below). The pyrite samples were first cleaned in acetone (2×30 min in an ultrasonicator) and then etched for 2×30 s. with sulphuric acid. SEM characterisation showed that fine particles, which initially adhered to the smooth pyrite surfaces, were removed. Similar to the experiments described earlier, mackinawite was aged for 168 h in a reduced environment (50% H_2S/H_2 mixture) before adding the pyrite nuclei. Thereafter, the pyrite cubes were dropped into the reaction vessel through one of the ports, while the flow rate of the reduced gas was increased in order to prevent oxygen from entering the system. In steps of 0.5 to 120 h, slurry samples were withdrawn and the reaction progress determined. After 5 days of equilibrating the seeds with the slurry, no additional changes in the solids were observed and then a slow oxidation process was induced while the pyritization reaction continued. At the end of the run, the surfaces of the pyrite cubes were examined with SEM techniques. The starting conditions and reaction products of all experiments are given in Tables 1 and 2.

3. Results and discussion

3.1. Ageing experiments

In all reduced experiments with $H_2S_{(aq)}$ as the sole sulphur source, the only solid product was crystalline mackinawite (Tables 1 and 2 and Fig. 3a,b). Under totally reduced conditions, regardless of variations in physical (temperature, time) and chemical (ΣFe^{2+}, ΣNa, $\Sigma S_{red(aq)}$, Eh, pH,) conditions, mackinawite did not react to pyrite under low temperature, acid to alkaline conditions. This is despite the high supersaturation of all experiments with respect to pyrite as shown in Fig. 2.

The nucleation of mackinawite is a fast process, and mackinawite is stable as long as the conditions are kept reducing and no other sulphur species of intermediate oxidation state are available. First XRD peaks (d-spacing 5.05, 2.97 and 2.31) for poorly ordered mackinawite can be observed after 5–30 min of reaction (Fig. 3a). These peaks become sharper and others develop with time. X-ray patterns of the solid products of experiments conducted for up to 4 months (2850 h, run A5) show that in environments where the only sulphur source is reduced aqueous H_2S or HS^-, mackinawite is the only stable low temperature iron monosulphide (Fig. 3a, Tables 1 and 2). The SEM photomicrograph (Fig. 3b) reveals ~ 100 μm platelets with a sulphur to iron ratio close to 1 (SEM-EDS determination). The size and morphology of these platelets resulted from aggregation of the colloidal suspension on the filter and the actual size of individual particles in suspension could not be assessed. An estimate of particle size, for dispersed FeS particles is given by Rickard (1997), who from XRD and SEM observations estimated an upper size limit of 35 nm.

The ageing experiments demonstrate that transformation of an iron monosulphide precursor, mackinawite, to more stable iron disulphides, pyrite or marcasite, requires an oxidant other than H_2S. In these experiments, the maximum content of chrome-reducible sulphur (i.e., FeS_2 and S^o) formed after 4 months was below 4–7%, thus within the limits of accuracy of the coulometric measurements. By XRD the detection limit of a phase is estimated to be $\sim 5\%$ and only mackinawite was found.

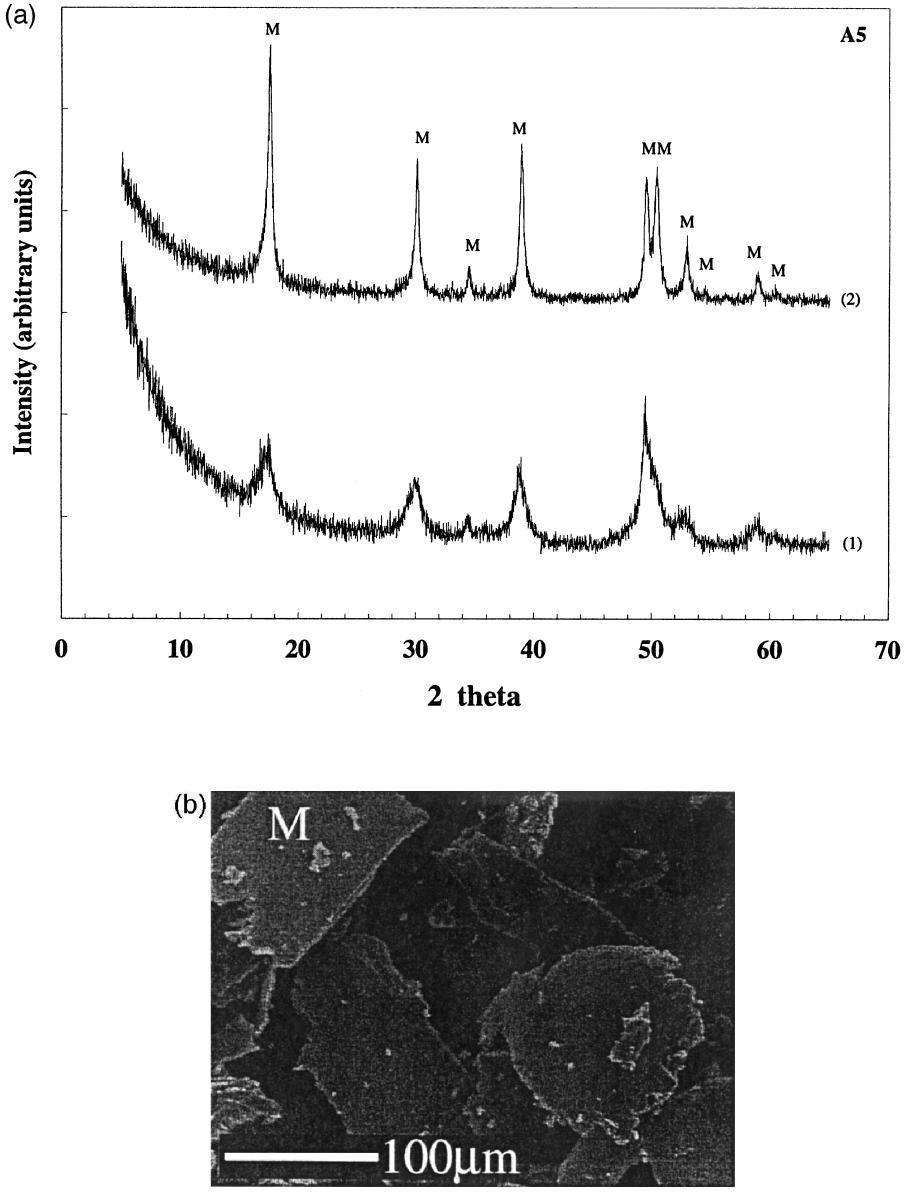

Fig. 3. (a) X-ray patterns for in situ precipitated mackinawite at 50°C (Run A5). (1) Pattern of in situ precipitated mackinawite (M) aged for 30 min in a pH = 4.6 H_2S solution with 99.5% H_2S gas overpressure. (2) Pattern of mackinawite aged for 2850 h under the same conditions as in (a). The crystallinity of the precipitate apparently increases with time. (b) Scanning electron microphotograph of aged mackinawite. The size of the particles, ~100 μm, and the observed texture are a consequence of filtering and does not represent the original texture of the dispersed mackinawite in solution.

Previous experimental data on pyrite formation pathways are contradictory. Numerous experimental studies have demonstrated that at temperatures below 100°C the conversion of unoxidized mackinawite to pyrite is a very slow process. It was shown that this is not an important process in low temperature pyrite formation (Berner, 1967, 1970; Roberts et al., 1969; Rickard, 1975; Taylor et al., 1979a,b; Murowchick

and Barnes, 1986; Schoonen and Barnes, 1991b; Wilkin and Barnes, 1996). These studies revealed that pyrite forms only when the precursor mackinawite is oxidised or when sulphur species of intermediate oxidation states, i.e., elemental sulphur or polysulphides, are involved in the reaction; thus, the formation of pyrite occurs via the 'polysulphide' pathway [Reactions (1)–(2)]. Nevertheless, the 'H_2S'-pathway, [Reaction (3)], has been proposed as the fastest pyrite-forming pathway (Wächtershäuser, 1988, 1993), and this pathway has received support from experimental studies (Drobner et al. 1990; Rickard 1997). Drobner et al. (1990), using in-situ precipitated FeS (experiment 3a, in their Table 1), showed at 100°C, that the conversion to pyrite is occurring, but not going to completion, i.e., mackinawite is still present even after 14 days (336 h). When pyrrhotite was used as precursor phase (experiments 1 and 2 in their Table 1 and XRD-patterns in their Fig. 1) only minor amounts of pyrite formed but reaction rates were not given. However, in a detailed experimental study, Rickard (1997) suggested that mackinawite in a H_2S solution reacted completely to pyrite within 48 h at 25°C to 125°C. These experiments will be discussed later because of the different precursor starting material, freeze-dried mackinawite.

The disagreements between the experimental results described above have triggered the long term ageing experiments described here. Previous experiments (Berner, 1967; Rickard, 1969, 1975; Taylor et al. 1979a,b; Schoonen and Barnes, 1991a,b,c; Wilkin and Barnes, 1996) were designed mostly to explore the conversion mechanisms of mackinawite to pyrite. None of these experiments was designed to determine the stability of mackinawite. In this study, mackinawite has been proven to be stable for up to 4 months as long as reducing conditions are maintained, and over this period, the conversion to pyrite does not occur via the 'H_2S-pathway'. However, an evaluation of the mechanism of pyrite nucleation and growth was not an objective of this study. These new experiments have shown that in reducing H_2S and HS^- solutions, pyrite forms at a negligible to very slow rate. In order to qualitatively verify the effects of oxidation on the stability of mackinawite various tests were conducted (see below). In addition, the stability of mackinawite demonstrated in the ageing experiments provided an ideal basis for determining the solubility of mackinawite at 25°C to 95°C (see below).

3.2. Controlled oxidation experiments

Induced oxidation experiments were carried out in an attempt to better understand the effects of oxidation on the rates of pyritization. In contrast to the experiments described above, in the 'induced oxidation' experiments, depending on the extent of oxidation, additional phases formed including greigite, pyrite, sulphur, goethite, and hematite.

In the 'slow oxidation' experiments the quantitative decrease (Fig. 4a, run SO12) and disappearance (Fig. 4b, run SO9) of mackinawite and the concomitant formation of greigite and pyrite, were interlinked with the appearance of elemental sulphur. The presence of sulphur indicates that the reduced aqueous sulphur species (H_2S and HS^-) were at least partly oxidised. Depending on the pH of the solutions, pyrite formation was accompanied by the formation of aqueous polysulphide species, indicated by the colour change of the supernatant solutions, from near colourless to yellow. In Fig. 4a, after 240 h of slow oxidation, the transformation to pyrite is incomplete, and mackinawite and greigite persist. In addition, two experiments at very alkaline pH (pH $\sim$ 12, SO8 and SO13) illustrated that even when 'slow oxidation' was induced for $>$ 2500 h, mackinawite remained the stable phase. Similar slow conversion rates occurred in run SO7, when one port of the reaction vessel was open to air but the vapour space above the mackinawite slurry was saturated with a mixture of 10% H_2S, thus slowing down the oxidation process. In this experiment, even after 468 h, less than 13% of the initial mackinawite transformed to pyrite. However, in most experiments, longer time intervals (i.e., 579 h and 939 h, Fig. 4b, run SO9) gave complete conversion to pyrite with all other precursor phases reacted.

In these experiments, although greigite was consumed (as indicated by the XRD scans) the magnetic character of the solids was retained. Pyrite is not magnetic, so any magnetic character indicates that cores of the newly formed pyrite are remnants of the precursor magnetic greigite, thus the conversion from mackinawite via greigite to pyrite was a solid state

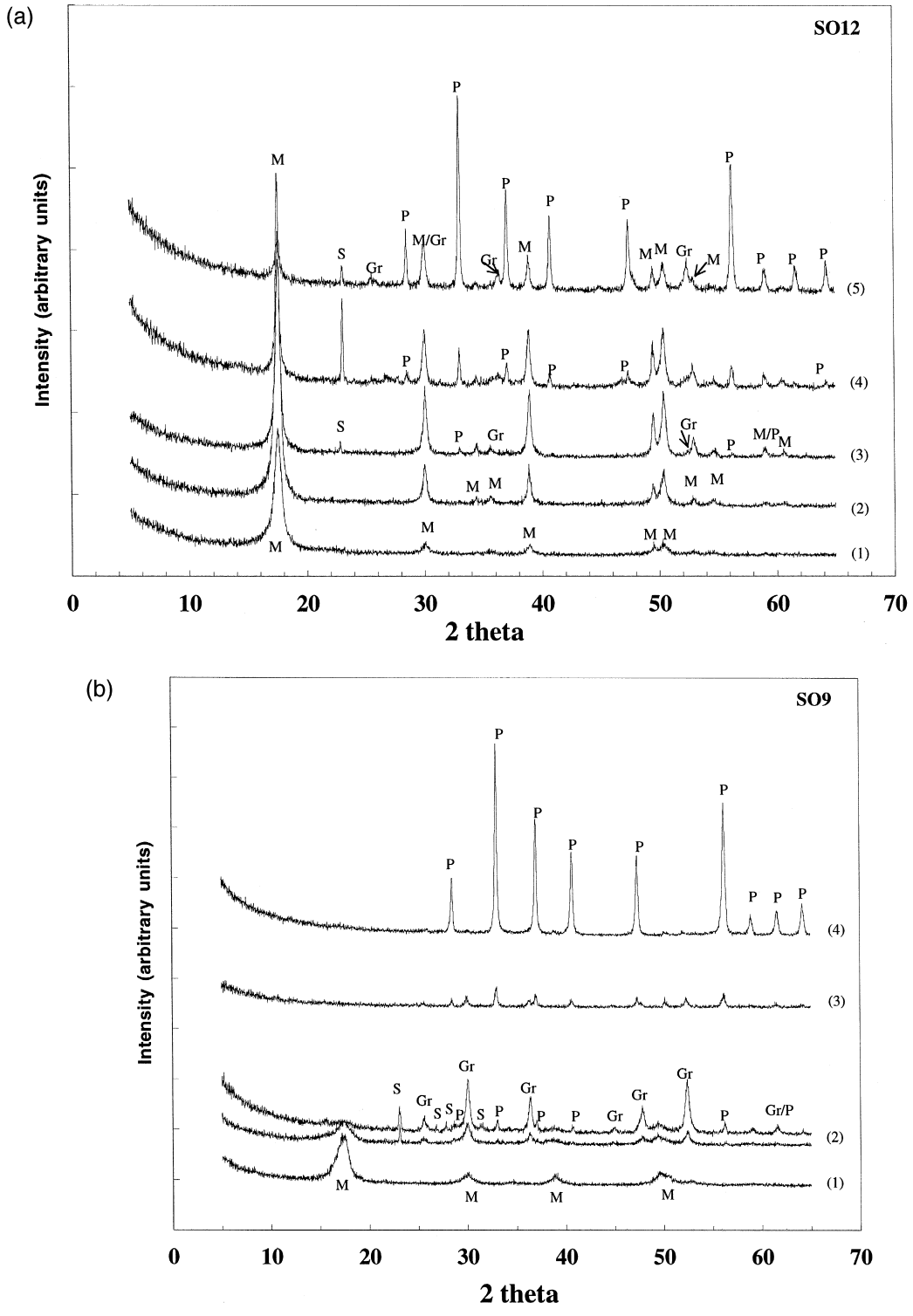
(a)
SO12
Intensity (arbitrary units)
2 theta
(5)
(4)
(3)
(2)
(1)
(b)
SO9
Intensity (arbitrary units)
2 theta
(4)
(3)
(2)
(1)

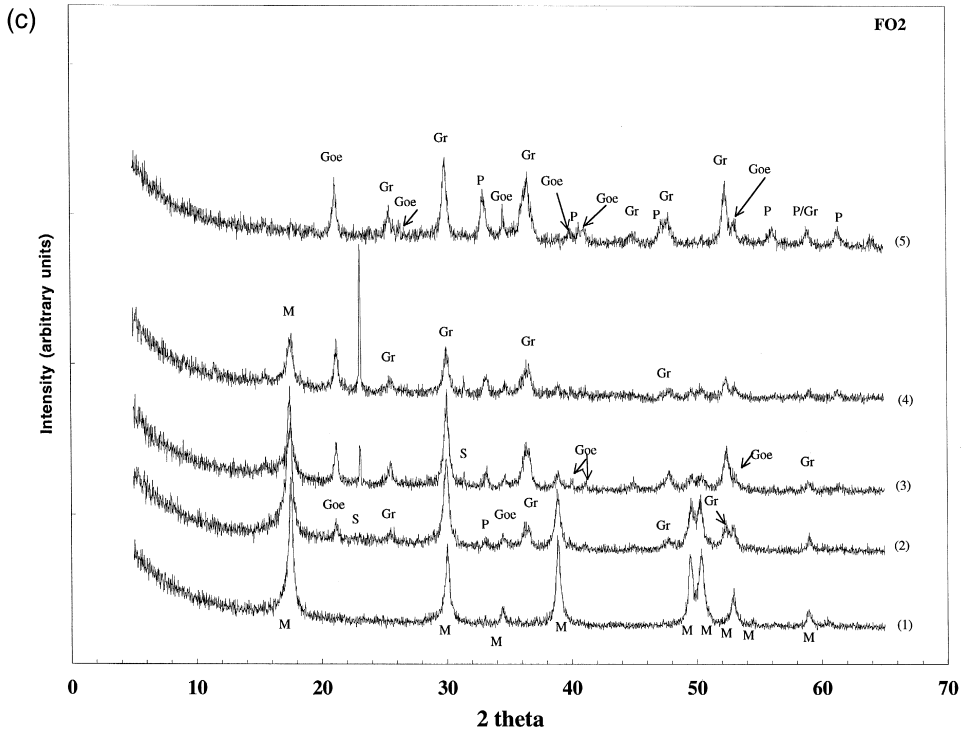

Fig. 4. (a). Diffraction patterns obtained during the low pH, slow oxidation run SO12 at 95°C. In all following figures with XRD patterns, the *Y*-axis represents intensity and a relative non-linear time axis. The bottom pattern always represents the starting material (i.e., pure mackinawite), while the above patterns represent increasing time intervals and oxidation conditions. In addition, the constituent phases of the first and last scans are fully labelled, while on the intermediate scans only the newly formed phases are labelled (M = mackinawite; Gr = greigite; P = pyrite; S = sulphur; Goe-goethite). (1) In-situ precipitated and aged for 1 h in a pH = 3.6 solutions with H_2S gas. (2) Same as above, but aged for 172 h. (3) H_2S-gas flow stopped for 24 h, pH = 3.69, solids magnetic. (4) H_2S-gas flow stopped for 98 h. (5) H_2S-gas flow stopped for 240 h. (b) Diffraction patterns obtained during the high pH, slow oxidation run SO9 at 80°C. (1) In-situ precipitated and aged for 96 h in a pH = 7.39 sulphide solution under 50% H_2S gas. (2) No gas overpressure for 70 (lower scan) and 75 h (lower scan), pH = 7.31 and 7.91, solids magnetic. (3) Aged for 579 h with no gas overpressure, pH = 8.83, solids magnetic. (4) Aged for 939 h with no gas overpressure, pH = 6.96, full conversion to pyrite, solids not magnetic. Labelling is the same as in (a) (see text for details). (c) Diffraction patterns obtained during the low pH, fast oxidation run FO2 at 75°C. (1) In-situ precipitated and aged for 144 h in a pH = 3.9 H_2S solution with 50% H_2S gas overpressure. (2) 35 min air bubbled through solution, pH = 6.1, solids magnetic. (3) Aged for 3 h as below and with additional 30 min air, pH = 5.4, solids magnetic. (4) 8 h and an additional hour air later, pH = 4.5, solids magnetic; (5) 24 h later, pH = 4.5, solids magnetic. It required an additional 185 h to full conversion to pyrite, although the solid fraction was still magnetic. In addition, minor goethite was observed, mostly at the solution glass interface. Final XRD patterns correspond to the uppermost scans in (b) and Fig. 6a. Labelling is the same as in (a) (see text for details).

process. Lennie et al. (1997) and Herbert et al. (1998) discussed the transformation of mackinawite to greigite in experiments conducted with dry mackinawite powder. A comparison between the current results and their experiments is difficult as different conditions applied. However, they concluded that oxidation promotes the formation of a Fe^{3+} enriched outer layer on the mackinawite surface, and subsequently the solid state transformation to greigite.

In the fast oxidation experiments (FO-runs), when a well-aged mackinawite slurry was intentionally oxidised, the transformation of the mackinawite suspension to pyrite also occurred, but at a faster rate. This conversion path involved similar intermediate solid phases (greigite and elemental sulphur) but in addition, iron oxides and oxyhydroxide species (goethite and hematite) formed. Run FO2 (Fig. 4c), started with a mackinawite slurry aged for 144 h

with a high $Fe^{2+}/H_2S_{(aq)}$ ratio, through which air was bubbled for 35 min. The initial pH of 3.9 instantly increased to 6.1 and goethite, greigite, sulphur and pyrite formed. Over the next 24 h and with additional air, the pH dropped to a value of 4.5, mackinawite and sulphur were consumed and the relative amounts of the other phases changed. However, it takes an additional 185 h to complete the transformation to pyrite. Although the final X-ray pattern did not indicate the presence of goethite, on the walls of the glass reactor, at the interface between the slurry and the vapour space, a thin brown-yellow layer of goethite was observed. The initial oxidation of aqueous ferrous iron to ferric iron promoted faster formation of goethite. In addition, sulphur was formed by oxidation of H_2S, and thus promoted the oxidation of the mackinawite precursor to greigite via a solid state transformation (Wilkin and Barnes, 1996; Lennie et al. 1997; Herbert et al. 1998). At more alkaline pH values polysulphide species formed, shown by the yellow colour of the filtered solutions. In Fig. 5a–c, the photomicrographs of different reaction products are presented. A more quantitative comparison with the anoxic runs and literature data is given at the end of the freeze-dried section.

In these experiments the reactive species responsible for driving pyrite formation is unresolved because a mixture of O_2 and aqueous sulphur species with intermediate oxidation states were present, either of which could be important for pyrite formation. The key conclusion, however, is that some degree of oxidation is required for mackinawite to react to pyrite.

3.3. Freeze-dried experiments

During the course of these experiments extreme care was taken to exclude oxygen. However, the freeze-drying procedures potentially could allow for oxidation of the precursor mackinawite. This is particularly true for the ex situ freeze-dried materials, where partial oxidation could not be fully prevented during anaerobic freeze-drying and re-equilibration. This concern was justified by previous studies that have shown that even slight oxidation will permanently change the surfaces of mackinawite (Taylor et

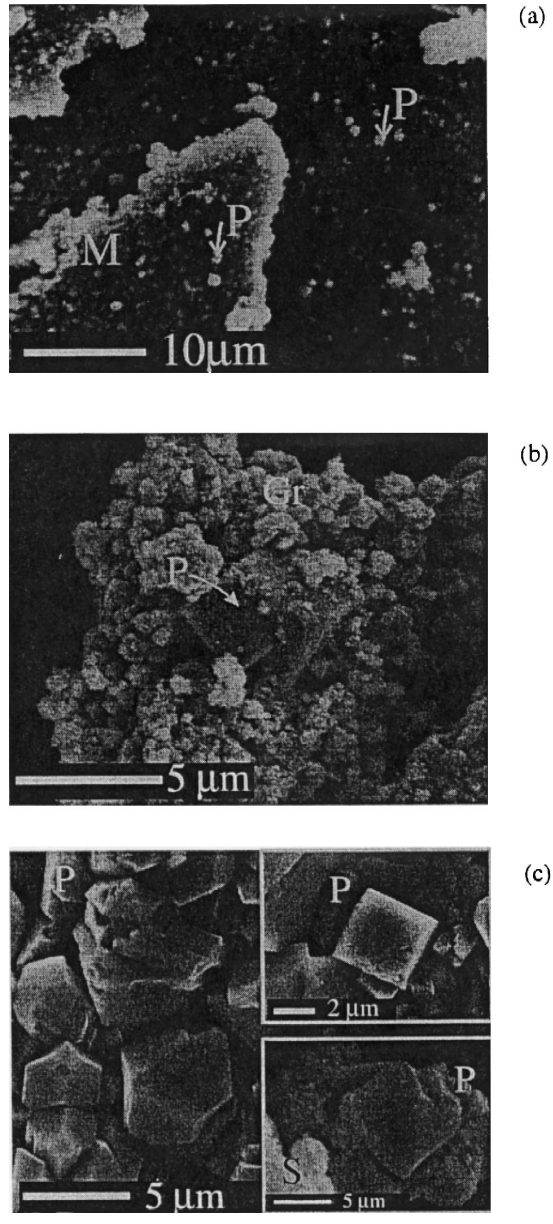

Fig. 5. Scanning electron microphotograph of reaction products during the controlled oxidation experiments. (a) Mackinawite platelets with pyrite grains smaller than 1–3 μm, grown during slow oxidation; the material was magnetic indicating that greigite acted as a precursor to pyrite. (b) Greigite and pyrite grains produced in the late stages of a slow oxidation experiment. (c) Pyrite morphologies obtained at the end of long-term slow and fast oxidation experiments. Note that cubes, octahedra, and pyritohedra are present.

al., 1979a,b; Wilkin and Barnes, 1996; Lennie et al., 1997; Herbert et al., 1998). In addition, although mackinawite is far more reactive than the more stable pyrrhotite and pyrite, exposure of pyrrhotite to oxygen (Pratt et al., 1994) or of pyrite to water or oxygen (Guevremont et al., 1998) resulted in very fast oxidation of the surfaces of these minerals.

Before freeze-drying, the aged monosulphides were sampled and XRD of the ink-black precipitate gave pure mackinawite patterns. After freeze-drying, the material consisted of a mixture of ink-black, very fine mackinawite partly mixed with white fluffy crystals of an unidentified ammonium-sulphate salt apparently produced from the Mohr's salt used in the preparation procedure. These salts dissolved readily after re-equilibration with fresh H_2S solution. The amount of this salt in the freeze-dried samples was below the 5% detection limit of the X-ray method and the patterns revealed only mackinawite peaks (Fig. 6a, second scan from bottom). Microscopic evidence, however, showed distinct morphology changes between the freeze-dried samples (Fig. 6b) and the aged material (Fig. 3b). Observed was a mixture of fuzzy, clumped needles, filigree-like forms, and small clusters and aggregates of FeS composition (SEM-EDX-determination). However, after re-equilibrating the freeze-dried samples with fresh H_2S solution, and sampling again, the SEM photomicrographs of the filtrate revealed platy characteristics similar to aged mackinawite particles. Thus, presumably after re-equilibration, the character of the suspension was restored to the pre-freeze-dried conditions.

The surface area of the ex-situ freeze-dried material was measured using BET techniques. Nitrogen and krypton gas were used, and the results are reported in Table 3, together with literature data on estimated and measured surface areas for mackinawite. The measured surface area of the freeze-dried material from the current study, 16–21 m^2/g, lies within the range of previously reported values. Rickard (1975) estimated a surface area for the precursor FeS phase of ~ 44.4 m^2/g (1.6×10^5 $cm^2/0.36$ g) while Taylor et al. (1979b) reported a BET surface area for freshly precipitated mackinawite of 7 m^2/g. From particle size estimates, Rickard (1997) calculated the limiting geometric surface area for dispersed FeS to lie between $39 m^2/g$ and 136 m^2/g. The same author, who used freeze-dried mackinawite in his experiments but possibly performed the BET measurements on fresh material, later confirmed this estimate. The BET measurement yielded a surface area for mackinawite of 36.5 m^2/g. Widler (1999) reported BET surface areas for fresh mackinawite of 80–82 m^2/g, thus within the limits of the estimates of Rickard (1997).

The large differences in calculated or measured surface areas are, however, not surprising. BET surface area measurements crucially depend on grain size and state of aggregation, and thus preparation of the sample, while estimates rely on an initial assumption of particle size. In this study, the freeze-dried material was ground under acetone in a glove box and thus it was assumed that the material was well dispersed. However, the morphology and structure observed on the freeze-dried mackinawite might indicate a decrease in the total surface area in contrast to colloidal material of fresh precipitates.

The X-ray patterns in Fig. 6a show that at 25°C, when the re-equilibrated in-situ freeze-dried mackinawite was kept for 42 h under an overpressure of 100% H_2 (in these experiments lowest possible oxidation potential within the pyrite field), no change in solid phases was observed. Consequently, freeze-dried mackinawite, although potentially oxidised during the freeze-drying process, will persist for some time under highly reducing conditions because hydrogen gas is a strong reductant (at pH = 4.3, Eh = -0.254 V).

When the same suspension was equilibrated with H_2S (i.e., Eh ~ -0.186 V), the oxidation potential was raised higher in the pyrite stability field, and after 24 h peaks for sulphur appeared. The intensity of the mackinawite peaks decreased after 66 h and coulometric analysis revealed 64% pyrite. The solid product was magnetic indicating that greigite was a precursor to pyrite, although the X-ray patterns did not indicate its presence (Fig. 6a). However, the sensitivity was compromised because the two main peaks of greigite (d-spacing 2.98 and 1.75) overlap with those of mackinawite (2.97 and 1.73). This suspension was aged for 218 h with H_2S overpressure, and a 100% transformation of the initial mackinawite to pyrite was observed (uppermost pattern in Fig. 6a) and the magnetic character of the final fraction disappeared.

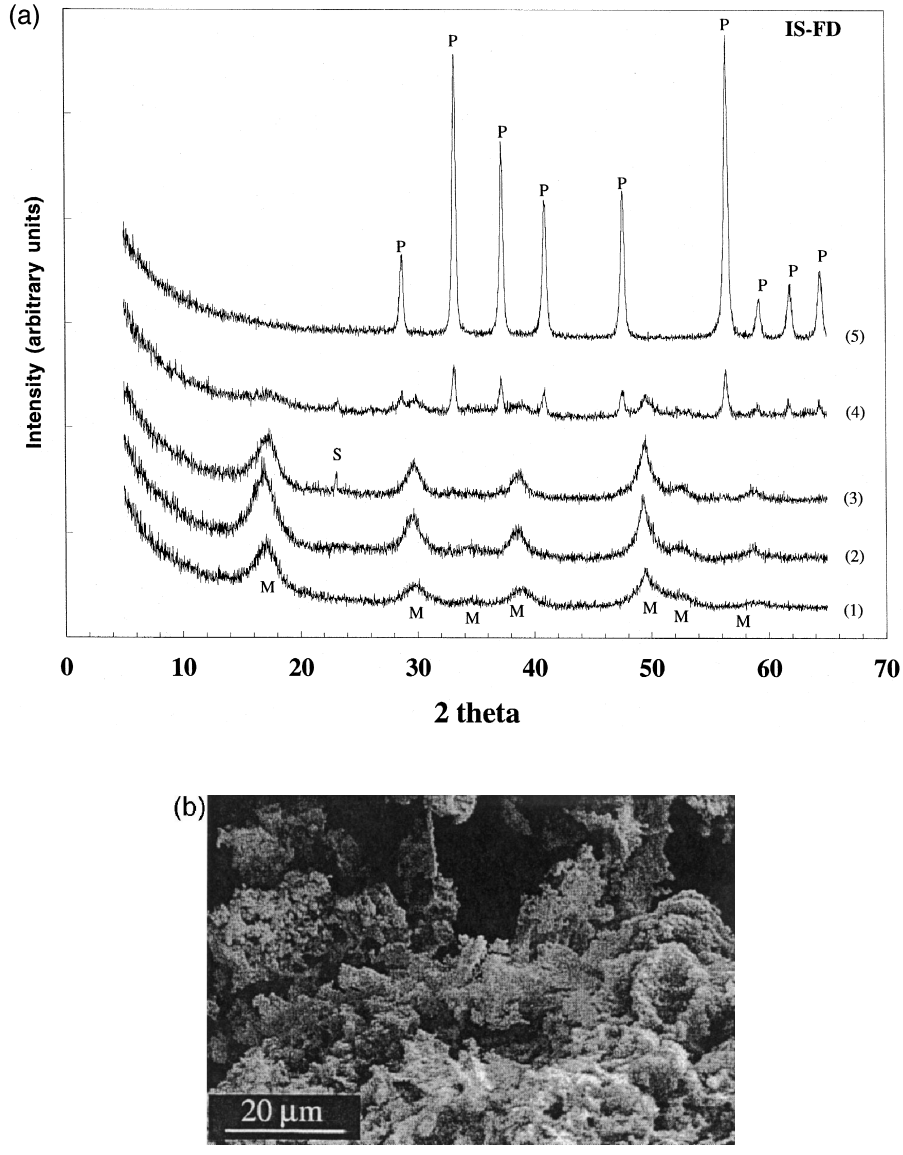

Fig. 6. (a) Diffraction patterns obtained with in-situ freeze-dried mackinawite re-equilibrated at 25°C with an H_2S solution and variable gas overpressures. (1) Aged for 72 h in a pH = 4.3, H_2S solution under 99.5% H_2S gas. (2) In-situ freeze-dried and consequently re-equilibrated and aged for 42 h in a 0.1 m H_2S solution under 100% H_2 gas. (3) Aged for 66 h in a 0.1 m H_2S solution under 99.5% H_2S gas; first sulphur peaks are visible. (4) Aged for 108 h under the same conditions as below, pH = 4.95, solids magnetic, 64% pyrite. (5) Aged for 216 h as below, pH = 6.3, solids not magnetic, 100% pyrite. Labelling is the same as for Fig. 4a. (b) Scanning electron microphotograph of ex situ freeze-dried mackinawite.

The results of the freeze-dried experiments are fundamentally incompatible with the observations from the in-situ ageing experiments, where even for much longer time periods the conversion of mackinawite to pyrite did not occur. However, the results agree well with the intentional fast oxidation experiments, as the transformation rates are similar. The observed transformation rates of the freeze-dried sulphides, however, were slower than the rates reported by Rickard (1997), who, at 25°C, observed within 24

Table 3
Surface areas (m^2/g) for various mackinawite precursor materials, from this study and from the literature

Source	Method	Surface area	Material
Rickard (1975)	estimated	~ 44.4 m^2/g	
Taylor et al. (1979b)	BET	7 m^2/g	fresh
Rickard (1997)	estimated	35–135 m^2/g	
Rickard (1997)	N_2 BET	36.5 m^2/g	fresh/freeze-dried(?)
Widler (1998)	N_2 BET	~ 80–82 m^2/g	fresh
This study	N_2 and Kr BET	16–21 m^2/g	freeze-dried

h a 60% conversion of the initial mackinawite to pyrite (Fig. 7). In the current study, within the first 24 h, no pyrite was observed and only after 60 h a 64% conversion was observed (Fig. 6a). A quantitative comparison with Drobner et al. (1990) is not possible as only qualitative conversion products were reported and different starting materials were used.

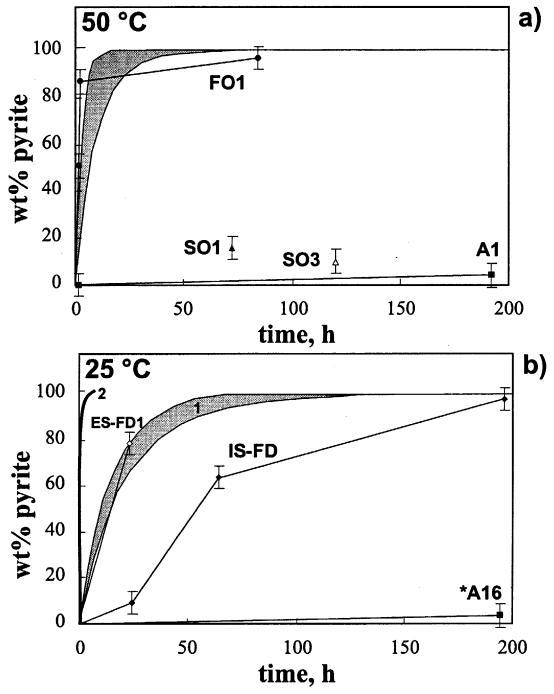

Fig. 7. Extents of reaction (wt.% pyrite) vs. time, calculated using the rate equation from Rickard (1997). (a) 50°C: shaded area represents the uncertainty zone calculated for 0.044 m FeS and 0.1 m to 0.03 m H_2S; small square: run A1; filled and open triangle: SO1 and SO3; filled circles: FO1; (b) 25°C: shaded area (1) is calculated for 0.041 m FeS and 0.1 and 0.15 m H_2S; line (2) calculated after Canfield et al. (1998); small square: run A16, (* total equilibration time was 336 h); open diamond: ES-FD1, filled diamonds: IS-FD (see Table 1 and text for details).

However, in their experiments, the full conversion to pyrite had not been observed even after 336 h, which is in general agreement with the slow oxidation experiments reported above, where after 216 h also only partial conversion was observed.

In contrast, the experiments conducted with ex-situ freeze-dried mackinawite show the conversion to pyrite occurring at a comparable or much faster rate than previously reported (Rickard, 1997). At 25°C, 78% of the initial ex situ freeze-dried mackinawite was transformed to pyrite, via greigite, within 24 h (Table 1 and Fig. 7), while at 100–200°C, this transformation occurs, within minutes to hours (Cahill et al., this issue; Benning et al. in prep). In comparison, at 100°C, Rickard (1997) showed that a freeze-dried precursor reacted within 1 h, 6 h, and 24 h to form 32%, 45% and 85% pyrite. Hence, it is believed that despite the efforts to avoid oxidation in the freeze-drying procedure, the ex-situ, as well as the in-situ freeze-dried material must have been oxidised.

The experiments with freeze-dried mackinawite indicate that increasing oxidation of the precursor phase also increases the rate of reaction. However, a quantification of this effect from the derived data is difficult.

A quantitative comparison with literature data can be made using the rate equation suggested by Rickard (1997):

$$\frac{d_{FeS_2}}{dt} = k(FeS)\left(cH_2S_{(aq)}\right) \quad (4)$$

where k is a second order rate constant (at 25°C $k = 0.371$ l mol/h; at 50°C, $k = 2.794$ l mol/h, Rickard and Luther, 1997), and (FeS) and $(cH_2S_{(aq)})$ are mol/l of solid precursor and aqueous H_2S, respectively. Conversion rates for selected experi-

ments from the current study and from literature, were calculated and are plotted in Fig. 7.

The chemical parameters ($FeS_{(s)}$ and $H_2S_{(aq)}$) for selected anoxic runs were taken as boundary values, and a predicted rate was calculated (shaded areas in Fig. 7a,b). The percent conversion for an ageing experiment as well as data for slow and fast oxidation runs (Fig. 7a) and freeze-dried mackinawite (Fig. 7b) were plotted for time periods up to 200 h. The percent conversion in the ageing runs (A1 and A16) is incompatible with the predicted rates. The calculated conversion rate predicts a completed reaction after maximum 75 h at 50°C (Fig. 7a) and 125 h at 25°C (Fig. 7b), compared with runs [A1] and [A16], where after 192 h and 326 h, respectively, a maximum of 4% and 5% pyrite were observed. Also plotted is the extent of conversion from the slow oxidation runs [SO1] and [SO3], where after 72 h and 120 h only 16% and 10% pyrite was observed. High conversion percent was observed when fast oxidation was induced [FO1]. After 1 h, 1.5 h, and 84 h, 51%, 87%, and 97% of the precursor material converted to pyrite, thus at a comparable rate with the predicted values (Fig. 7a). A better agreement is achieved when the freeze-dried experiments are compared with the predicted rates. In the in-situ freeze-dried experiment after 24 h, 66 h, and 218 h, 9%, 64%, and 100% pyrite was determined. The ex-situ freeze-dried mackinawite reacted much faster and after 24 h, 78% of the initial mackinawite was transformed to pyrite. These rates, bracket the predicted rate region and are comparable with the values obtained by Rickard (1997), indicating that the higher the oxidation of the material the faster the rate of conversion. Also plotted in Fig. 7a are pyrite formation rates estimated by Canfield et al. (1998), who used the rate equation suggested by Rickard (1997). Canfield et al. (1998) predicted that in reducing environments where the sulphur chemistry is governed by bacterial sulphur metabolism, the rate of pyrite formation is 10^4 to 10^5 faster than in inorganic experiments. They predict that all FeS transforms within seconds to tens of seconds to pyrite. However, in the inorganic experiments presented in this study such high conversion rates can only be explained with oxidation. In addition, in recent experiments performed under anaerobic conditions with sulphate-reducing bacteria and iron monosulphides, the conversion of pyrite did not occur even after 6 months. It could be shown that the sole role of the sulphate reducing bacteria was to provide the reduced sulphur source and that they did not play an active metabolic role in mineral conversion (Benning et al. 1999). The process of pyrite crystallisation follows an inorganic process not directly influenced by the activities of sulphate reducing bacteria. The observations of Canfield et al. (1998) also contradict the fact that in several natural environments, AVS (mackinawite, greigite) are observed to be stable in zones of high bacterial activity (Lyons, 1997; Wilkin and Barnes, 1997; Suits and Wilkin, 1998).

3.4. ''Seeding'' experiment

This experiment was designed to test whether in a reduced suspension of mackinawite, an oxidised surface of a pyrite seed would promote pyrite nucleation at a much faster rate than without seeds. Conceptually, in a supersaturated solution a pyrite surface should induce heterogeneous pyrite nucleation and growth even at low temperatures. The surfaces of the natural pyrite cubes (Navajun, Spain) had been exposed to atmospheric oxygen. Therefore, it was assumed that the oxide layer would react with the precursor mackinawite and the kinetic barrier to pyrite nucleation at low temperatures (Schoonen and Barnes, 1991a,b,c) might be surpassed,thus allowing surface pyrite nucleation and continued growth.

The Navajun pyrite cubes were dropped into an experiment where a mackinawite slurry had been aged for 168 h at 95°C, and a pH of 3.6. After 30 min, weak pyrite peaks (d-spacing 1.63 and 2.71) appeared on the X-ray scans and the coulometric method indicated $\sim 8\%$ chrome-reducible sulphur fraction, where before seeding $\Sigma S_{CrCl_2} < 5\%$. Thus, it was concluded that the oxidised pyrite surfaces triggered pyrite nucleation.

However, equivocation arises on whether nucleation occurred directly from solution on splinters formed during the drop or on the seed surfaces, or via a solid solution transformation, as in the intentional oxidation experiments. Support for the first possibility comes from the fact that the new pyrite did not have a magnetic character and XRD did not indicate the presence of sulphur. Two paths could account for the direct growth without the greigite precursor. Either the new pyrite nucleated on the

seed surfaces and not via solid state transformation of mackinawite (i.e., via greigite), or the solid state transformation was so fast that the remanent magnetisation due to the greigite precursor was lost during reaction. The absence of sulphur in the suspension, even with pyrite present, could be explained by the fast reaction rate, and/or the small fraction of sulphur needed for the first pyrite to form. In addition, the new pyrite formed at this stage exhibited only cubic morphology, thus copying the seed morphology. Hence, the evidence suggests that surface nucleation is the dominant mechanism for the formation of the first generation of pyrite in this experiment.

After a total of 120 h of equilibrating the seeds with the mackinawite slurry, a steady state level of ~12% pyrite was measured. Then, the flow of reduced overpressure gas was stopped and a slow oxidation process was induced. Subsequently, for an additional 216 h, the reaction was continuously monitored (Table 1, run SO2) and the pyrite fraction increased to a maximum of ~60% with greigite and sulphur peaks appearing, thus imitating the slow oxidation process showed in Fig. 4a. During this second stage, it was also observed that all three pyrite morphologies developed.

The purely cubic morphology observed in the first stage of the seeding experiment was inconsistent with the morphologies developed in the intentional, controlled oxidation experiments, where all three forms (cubes, rhombohedra, and pyritohedra, Fig. 5c) were observed together. This may indicate that initially pyrite nucleated on the seed surfaces and subsequently, the slow oxidation process served as a trigger for the solid solution transformation of the mackinawite from the slurry. Similar to the slow oxidation experiments, after 216 h only 60% of the initial mackinawite transformed to pyrite and the reaction was not complete. More seeding experiments are currently being conducted to better assess these questions.

3.5. The absence of marcasite

In all low pH experiments performed in this study, the only observed iron disulphide was pyrite; no marcasite was produced. However, Murowchick and Barnes (1986) have experimentally shown that at temperatures below 75°C, in low pH, polysulphide solutions ($pH < pK_{1,\ polysulphide}$), where neutral polysulphanes (H_2S_2 or H_2S_4) dominate the aqueous zero-valent sulphur speciation, marcasite forms predominantly over pyrite. In their experiments below pH 5, aqueous polysulphane species either were added directly or were formed by partial oxidation of H_2S and $S_2O_3^{-2}$. In acid solutions, this process proceeds via the disproportionation of thiosulphate and the formation of colloidal sulphur. At more alkaline pH values, sulphide oxidation produces HS_x^- and S_x^{2-} and thus promotes the formation of pyrite. The upper pH limit of marcasite formation corresponds with the pH where HS_2^- becomes dominant over $H_2S_2^o$ ($pK_1 \sim 5$). Murowchick and Barnes (1986) have discussed the presence of greigite and mackinawite as reaction products but grew marcasite and pyrite directly from solution presumably after nucleation via the conversion of a precursor monosulphide.

Schoonen and Barnes (1991b) reacted excess elemental sulphur with a suspension of iron monosulphides aged in a H_2S solution, and confirmed the observations of Murowchick and Barnes (1986) that marcasite forms at low pH. However, they showed that this reaction proceeded via the conversion of FeS precursors and not via the direct precipitation of marcasite from solution. Wilkin and Barnes (1996) have confirmed the observation for higher pH values where pyrite was the product. They have conducted experiments with FeS precursors equilibrated with thiosulphate, elemental sulphur and polysulphide species at near neutral pH values, below 100°C. Their experiments demonstrated that $S_2O_3^{2-}$ promotes the conversion of mackinawite to pyrite, when the precursor phase had been oxidised (run 1, their Table 2), while unoxidized FeS remains stable in a thiosulphate solution (run 4 and 15, their Table 2). However, they showed conclusively that polysulphides and elemental sulphur and not thiosulphate promote the reaction of mackinawite to pyrite.

Wei and Osseo-Asare (1996) reacted ferric iron with sulphide ions in low pH aqueous solutions and produced elemental sulphur and FeS as precursors to pyrite. However, they also failed to produce marcasite in low pH sulphide solutions.

In the oxidation experiments carried out in the current study (SO-and FO-runs, Table 1) marcasite was never observed, although the majority of experi-

ments were carried out at pH below 5 and the partial oxidation of $H_2S_{(aq)}$ by O_2 was promoted. Often, the formation of elemental sulphur was observed as a starting point for the formation of pyrite (Figs. 4 and 6). In addition, in experiments where due to oxidation the pH increased to more alkaline values (e.g., runs FO1–3, SO6, SO9) polysulphide formation was indicated by the colour change of the supernatant solutions from clear to yellow. However, the concentrations of these species were low in comparison to the initial concentrations of polysulphides used in the experiments of Murowchick and Barnes (1986) and Schoonen and Barnes (1991b). Chen and Morris (1972) and Chen and Gupta (1973) showed that the oxidation rate of hydrogen sulphide to polysulphide is pH dependent and slow at pH values below 5. It is, therefore, possible that the high initial concentration of these species in the experiments of Murowchick and Barnes (1986) and Schoonen and Barnes (1991b) promoted the formation of marcasite.

Consequently, the formation of marcasite is apparently dependent on both pH and polysulphide concentration as well as on temperature. Nucleation can be via the same FeS precursors as for pyrite, shown by a residual magnetic character of greigite, and subsequent growth directly from solution is proven both experimentally and by the typical euhedral forms observed in nature. Because of the common occurrence of marcasite, the minimum concentrations of polysulphide that permit its growth are of considerable interest. Although experimental data are insufficient to establish this lower limit, it can be estimated from general kinetic data (Lasaga, 1998). Where reactant concentrations are about below 10^{-5}–10^{-6} m, reaction rates typically become slow enough that equilibrium is not achieved. Examples are the saturation indices of carbonates as discussed by Langmuir (1997) and the supersaturation states of many species in groundwaters (Barnes and Clarke, 1969) where equilibrium is common above these concentrations and becomes increasingly rare at lower concentrations. This observation implies that marcasite forms both below pH 5 and at polysulphide concentrations greater than 10^{-5}–10^{-6} m.

3.6. Solubility of mackinawite

The solubility of crystalline mackinawite at temperatures below 100°C was determined using the data from the ageing experiments described earlier (Tables 1 and 4).

The dissolution of mackinawite reduced H_2S and HS^- solutions can be expressed as:

$$FeS(s) + H_2S(aq) = Fe^{2+} + 2HS^- \quad (5)$$

This reaction is based on the assumption that for the conditions of these experiments, 25°C to 95°C and $pH_{25°C} = 3.2$–8.2, the dominant aqueous iron and sulphur species are Fe^{2+} and H_2S and HS^-, respectively. Although a general dissolution reaction including iron hydrosulphide complexes would provide a better description of the overall dissolution reactions in the Fe–S system, the simplified Reaction (5) was adopted. This was based on the results of Davison (1991), Davison et al. (1999), Luther and Ferdelman (1993), Wei and Osseo-Asare (1995) and Mountain and Seward (1998), who showed that the concentrations of iron hydrosulphide complexes are insignificant in acidic solutions. At higher pH, only two experiments were carried out and for those cases, the iron hydrosulphide species will be discussed later.

The solubility equilibrium is written for the nominal, FeS, with unit activity assumed for the solid and the standard state of the aqueous species is the ideal 1 m solution. Thus, the equilibrium constant, $K_{eq,FeS}$, for Reaction (5) can be calculated from:

$$K_{eq,FeS} = \frac{(a_{HS^-})^2(a_{Fe^{2+}})}{a_{H_2S}} \quad (5a)$$

The values for the H_2S ionisation reaction:

$$H_2S(aq) \Leftrightarrow HS^- + H^+ \quad (6)$$

with the constant, K_{1,H_2S}, (Table 4) expressed as:

$$K_{1,H_2S} = \frac{a_{HS^-}a_{H^+}}{a_{H_2S_{(aq)}}} \quad (6a)$$

taken from Suleimenov and Seward (1997). Coupling this expression with that for total reduced sulphur:

$$m_{S,tot} = m_{HS^-} + m_{H_2S} \quad (7)$$

allows the activities of HS^- and H_2S to be expressed as a function of K_{1,H_2S}, pH, and $m_{S,tot}$:

$$a_{HS^-} = \left[\frac{K_{1,H_2S}\gamma_{H_2S}}{a_{H^+} + K_{1,H_2S}\gamma_{H_2S}}\right] m_{S,tot}\gamma_{HS^-} \quad (8a)$$

Table 4
Iron and sulphur concentrations, ionic strength and calculated equilibrium constants for mackinawite following Eqs. (9) ($K_{eq,FeS}$) and Eq. (12) (K_{FeS})

Run #	T (°C)	pH	∑Fe	a_{HS^-}	a_{H_2S}	I	pK^{a}_{1,H_2S}	log $K_{eq,FeS}$	log K^{b}_{FeS}
RF	25	4.45	5.60E−04	2.06E−05	6.98E−03	0.323	6.98	−10.86	3.10
A16	25	4.50	4.95E−05	2.64E−04	7.97E−02	0.341	6.98	−10.76	3.20
A1	50	4.28	2.34E−05	2.46E−04	6.48E−02	0.328	6.70	−11.07	2.33
A1a	50	4.51	2.14E−05	2.76E−04	4.27E−02	0.328	6.70	−10.83	2.57
A2	50	4.86	4.49E−05	1.17E−04	8.08E−03	0.355	6.70	−10.54	2.86
A2a	50	4.58	4.28E−05	5.65E−05	7.44E−03	0.323	6.70	−11.15	2.25
A4	50	4.54	6.95E−06	6.05E−04	8.74E−02	0.300	6.70	−10.94	2.46
A10	75	4.52	5.03E−05	4.16E−05	4.36E−03	0.327	6.54	−11.13	1.95
A7[c]	80	*8.15*	3.05E−06	6.64E−03	1.56E−04	0.280	6.52	*−6.49*	*6.55*[c]
A12[c]	80	*7.39*	1.15E−05	5.37E−02	7.25E−03	0.182	6.52	*−5.73*	*7.31*[c]
A8	80	3.24	7.76E−03	3.93E−06	7.50E−03	0.907	6.52	−11.26	1.78
A9	90	3.86	1.20E−03	3.27E−06	1.40E−03	0.304	6.49	−11.48	1.50
A15	95	3.60	1.95E−04	1.71E−05	1.30E−02	0.187	6.48	−11.76	1.20

[a] Data from Suleimonov and Seward (1997).
[b] Calculated via Eq. (11a) and plotted in Fig. 8.
[c] Experiments at alkaline pH, assumed $\sum Fe = mFe^{2+}$.

and

$$a_{H_2S} = \frac{\left[\frac{K_{1,H_2S}\gamma_{H_2S}}{a_{H^+} + K_{1,H_2S}\gamma_{H_2S}}\right] m_{S,tot} a_{H^+}\gamma_{HS^-}}{K_{1,H_2S}} \quad (8b)$$

These expressions combined with the dissolution reaction for FeS [Eq. (5a)] provide an equation for the equilibrium constant $K_{eq,FeS}$ dependent only on $m_{Fe,tot}$ (here assumed to be equal to $m_{Fe^{2+}}$), pH and total sulphur, which were measured quantities given in Tables 1 and 4:

$$K_{eq,FeS} = \left[\frac{K_{1,H_2S}\gamma_{H_2S}}{a_{H^+} + K_{1,H_2S}\gamma_{H_2S}}\right] m_{S,tot}\gamma_{HS^-} m_{Fe^{2+}}\gamma_{Fe^{2+}} \times (a_{H^+})^{-1} K_{1,H_2S} \quad (9)$$

The aqueous activity coefficients of Fe^{2+} and HS^- were calculated by means of the Davies equation (Davies, 1962):

$$\log\gamma_i = -1.82492 \times 10^6 \rho_0^{1/2} (\varepsilon T)^{-3/2} \times z_i^2 \left(\frac{\sqrt{I}}{1+\sqrt{I}} - 0.31\right) \quad (10)$$

with the density and dielectric constant (ρ and ε) calculated after Haar et al. (1984). The activity coefficients for H_2S were calculated using the Henry's law constants of Suleimenov and Krupp (1994). In Table 4 for each experiment, the run number, temperature, $pH_{25°C}$, solution composition, ionic strength, and calculated equilibrium constants are given. In order to compare with equilibrium constants from the literature (Berner, 1967; Davison, 1991; Schoonen and Barnes, 1991b; Bågander and Carman, 1994; Davison et al. 1999) the equilibrium constant, K_{FeS} for the reaction:

$$FeS(s) + 2H^+ \Leftrightarrow Fe^{2+} + H_2S(aq) \quad (11)$$

have been calculated by combining reactions (9) and (6a):

$$K_{FeS} = K_{eq,FeS} - (K_{1,H_2S})^2 \quad (11a)$$

The values for this equilibrium constant are plotted vs. $1/T$ in Fig. 8, together with the literature data. Also shown in this figure is the best-fit line through all low pH equilibrium constants and the temperature dependent equation:

$$K_{FeS} = 2848.779/T - 6.347 \quad (12)$$

where T is in Kelvin.

The equilibrium constants determined here agree well with Davison (1991) who recalculated the 25°C stability constants for amorphous FeS, mackinawite, and greigite, from the data of Berner (1967), Tewari et al. (1978) and Kolthoff and Griffith (1938). In addition, Davison et al. (1999) provided a new experimental value at 25°C for the above reaction, which agrees well with the previous values. The difference between the three studies for mackinawite is $\sim$0.3 log units, thus within the uncertainties of the three experimental studies. This difference may be due to the mackinawite of the current study, which was aged longer than in the other studies, thus, was more crystalline and could have a slightly lower solubility. The field-based, low temperature (12.8°C to 18.8°C) equilibrium constants for amorphous mackinawite determined by Bågander and Carman (1994), although spread over a wider range, are also in good agreement. However, their data are from near neutral pH, where hydrosulphide species may become important although they were not considered. At higher temperatures, only one study is available (Schoonen and Barnes, 1991a, their Fig. 2). Using a high-temperature titration method, these authors showed that the solubility of their initial precipitate (amorphous FeS) does not change from 100°C to 250°C, where $\log K$ remains at 2.9 ± 0.2. Their value compared with the value at 95°C for aged mackinawite from this study (Fig. 8) diverges in the right direction, although the difference is larger than expected.

The molar Gibbs free energy for Reaction (11) can be calculated directly from the equilibrium constants derived from Eq. (12) following the expression:

$$\Delta G_r^o = -RT\ln K_{FeS} \quad (13)$$

where R is the gas constant (8.3141 J/K mol). For a linear temperature dependent reaction, the first derivative of Eq. (12) with respect to temperature provides a constant enthalpy, ΔH_r^o, while the second derivative, the heat capacity, $\Delta C_{p,r}^o$, is zero. In turn

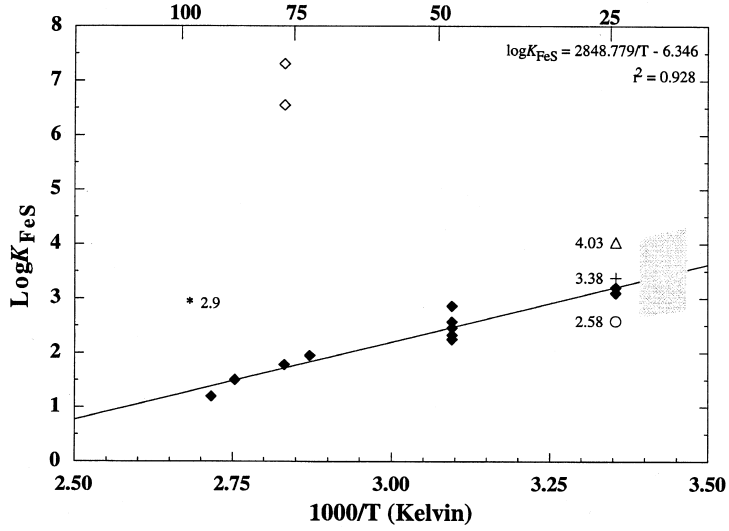

Fig. 8. Equilibrium constants, K_{FeS}, referring to Eq. (12) plotted as a function of inverse temperature, in Kelvin; the upper legend is in °C. The size of the symbols is larger than the estimated uncertainties of the calculated constants. Diamonds are experiments carried out in this study: solid diamonds at pH < 5; open diamonds at pH > 7 and 80°C (Table 3). The open circle, cross and triangle at 25°C are the values for greigite, mackinawite and amorphous FeS, respectively, from Davison (1991); the dotted area represents the range of data from Bågander and Carman (1994); the star marked 2.9 represents the value of Schoonen and Barnes (1991b); details see text.

the entropy, ΔS_r^o, can be calculated from ΔH_r^o and ΔG_r^o and is also constant. The functions calculated from 25°C to 100°C are summarized in Table 5. Using the ΔH_r^o and ΔG_r^o values at 25°C, the formation constants for mackinawite were calculated and are presented in comparison to literature data in Table 6.

In Fig. 8 it is obvious, that the two data points at 80°C are not compatible with the overall trend.

Table 5
Equilibrium constants and thermodynamic functions for the dissolution of mackinawite between 25°C to 100°C
$R = 8.3141$ J/K mol.
$\Delta G_r^o = -2.303RT\log K_{FeS}$.
$\Delta H_r^o = -2.303R * 2848.779$.
$\Delta S_r^o = (\Delta H_r^o - \Delta G_r^o)/T$.

Temp. (°C)	log K_{FeS}^a	ΔG_r^o (kJ/mol)	ΔH_r^o (kJ/mol)	ΔS_r^o (kJ/mol)
25	3.21	−18.31 ± 1.1	−54.55	−122
50	2.47	−15.27 ± 1.9	−54.55	−122
75	1.84	−12.24 ± 1.3	−54.55	−122
80	1.72	−11.63 ± 1.3	−54.55	−122
90	1.50	−10.41 ± 1.4	−54.55	−122
100	1.29	−9.20 ± 1.4	−54.55	−122

[a] $\log K_{FeS} = 2848.779/T - 6.347$.

These two experiments were carried out at higher pH, thus indicating that at these pH values, Fe^{2+} is not the dominant ferrous species, but instead an iron hydrosulphide complex is probable. However, both the stoichiometry and stability of the dominant iron hydrosulphide species in alkaline pH solutions are controversial. Two main species have been proposed: $FeHS^+$ and $Fe(HS)_2^o$. Wei and Osseo-Asare (1995) determined from spectrophotometric measurements the value for the formation constant of $FeHS^+$, $\beta_{FeHS^+,25°C}$ to be 4.5, while Luther and Ferdelman (1993) and Luther et al. (1996), using voltametric methods determined $\beta_{FeHS^+,25°C,seawater} = 5.2$ to 5.5. In contrast, Davison et al. (1999) found that $FeHS^+$ has an insignificant effect on the overall solubility and that in experiments at pH between 3 and 8, the best fit was achieved with $Fe(HS)_2^o$ with the formation constant $\beta_{Fe(HS)_2^o,25°C} = 6.45 \pm 0.12$. Mountain and Seward (1998) and Mountain (personal communication, 1999) consider the species $FeHS^+$ to be important only in a very restricted pH range (slightly below neutrality), while the species $Fe(HS)_2^o$ will be dominant in near neutral to alkaline solutions. The available data in Fig. 8 are insufficient to determine the iron sulphide speciation at high pH values. How-

Table 6
Gibbs free energy of formation and enthalpy of formation at 25°C for various iron sulphides

	$\Delta G^{o}_{f,\,298.15}$ (kJ/mol)	$\Delta H^{o}_{f,\,298.15}$ (kJ/mol)
Pyrite (FeS_2)[a]	−160.23	−171.64
Troilite (FeS)[a]	−101.33	−100.96
Greigite (Fe_3S_4)[b]	−290.4	–
recalculated[c]	−273.8	
Mackinawite (FeS)[b]	−93.3	–
recalculated[c]	−87.7	
amorphous FeS (FeS)[b]	−89.1	–
recalculated[c]	−83.7	
Mackinawite (FeS)[d]	−88.43	−74.30

[a] Robie et al. (1978).
[b] Berner (1967).
[c] Recalculated after Berner (1967), but using thermodynamic data for H_2S(aq) from Robie et al. (1978) instead of S^{2-}, because of the negligible activity of this species in natural waters (Giggenbach, 1971).
[d] This study; calculated using the values for mackinawite at 25°C from Table 4 and the Gibbs free energies of formation for Fe^{2+} (−78.87 kJ/mol) and H_2S (−27.87 kJ/mol) and the enthalpy of formation for Fe^{2+} (−89.10 kJ/mol) and H_2S (−39.75 kJ/mol) from Robie et al. (1978).

ever, in the absence of high temperature formation constants for iron hydrosulphide complexes, the formation constants for β_{FeHS^+} and $\beta_{Fe(HS)^o_2}$ at 80°C were estimated. It is expected that, similar to Au^+, Cu^+, Zn^{2+} and Pb^{2+} -hydrosulphide complexes (Giordano and Barnes, 1979; Bourcier and Barnes, 1987; Renders and Seward, 1989; Mountain and Seward, 1999), the formation constants will decrease or remain constant with increasing temperature. Decreasing stability with increasing pH is also expected, based on the slopes of the $FeHS^+$ and $Fe(HS)^o_2$ complexes in a concentration vs. pH space (slope = −1, for the monovalent cationic charged species and zero, thus indicating the lowest solubility for the uncharged species). The data for the higher pH values gave constants in disagreement with the expected higher temperature trends. The comparison with the literature data at 25°C for $FeHS^+$ (4.5 to 5.5) and $Fe(HS)^-_2$ (6.45) shows, that, in both cases the calculated log β (7.1 ± 0.2 for $FeHS^+$ and 8.8 ± 0.7 for $Fe(HS)^o_2$) increase with temperature. This suggests that in alkaline pH solution another negatively charged complex with a positive slope in the concentration vs. pH field must be dominant [$Fe(HS)^-_3$?]. However, additional data on the solubility of mackinawite at high pH and below 100°C are desperately needed.

4. Conclusions

Experiments conducted below 100°C in reducing sulphide solutions, showed that mackinawite is stable as long as no reactant other than H_2S is provided. Only oxidation of the precursor solid phase or of the reduced aqueous sulphur species promotes changes in solid and solution chemistry, and, thus favours the formation of intermediate iron monosulphide species and subsequently of pyrite.

Ageing experiments conducted for > 2800 h demonstrate that mackinawite suspensions, although supersaturated with respect to pyrite, do not convert to pyrite. Slow and fast oxidation experiments as well as experiments conducted with freeze-dried mackinawite and pyrite seeds show that pyrite formation occurs only after oxidation is induced. Furthermore, it can be concluded that the rates of transformation to pyrite increase with increasing degree of oxidation. These observations, however, imply a mechanism, which demands oxidised intermediate sulphur species (elemental sulphur, polysulphides) and/or surface oxidised monosulphide species (oxidised mackinawite, greigite), and therefore the 'oxidation' due to H_2S alone can be ruled out.

Although most experiments were carried out in low pH solutions, due to the low concentration of sulphide species with intermediate oxidation-state no marcasite was formed. It is concluded that pH alone will not drive marcasite formation, but that, in addition, a critical threshold in the concentration of the intermediate sulphur species needs to be reached before marcasite can form.

From the long term ageing experiments the solubility of mackinawite to 100°C has been measured. From these measurements, the high temperature equilibrium constants, as well as the thermodynamic reaction and formation functions for mackinawite were calculated. At 25°C a good agreement with literature data is achieved and with increasing temperatures, the solubility increases.

These data have implications towards the understanding of the reactions occurring in anoxic sedimentary basins where monosulphides and disulphides form under similar conditions. In such environments, the availability of oxidised sulphur and iron species with depth, will control the degrees of oxidation and in turn these factors will govern the rate of conversion of monosulphides to pyrite.

Acknowledgements

Financial support from the National Science Foundation grant number EAR 95-26762 is gratefully acknowledged. We wish to thank Henry Gong from the Pennsylvania State Materials Characterisation Laboratory for the analytical support provided during the entire study. In addition, we want to thank M. Schoonen and an anonymous reviewer for valuable comments, which clearly improved the quality of the paper.

References

Allen, E.T., Crenshaw, J.L., Johnson, J., Larsen, E.S., 1912. The mineral sulphides of iron with crystallographic study. American Journal of Science 23, 169–236.

Atkin, B.P., Sommerfield, C., 1994. The determination of total sulphur in geological materials by coulometric titration. Chemical Geology 111, 131–134.

Bågander, L.E., Carman, R., 1994. In-situ determination of the apparent solubility product of amorphous iron sulphide. Applied Geochemistry 9, 379–386.

Barnes, I.K., Clarke, F.E., 1969. Chemical properties of ground water and their corrosion and encrustation effects on wells. U.S. Geological Survey Professional Paper 498D, 58.

Benning, L.G., Barnes, H.L., 1998. In situ determination of the stability of iron monosulphide and kinetics of pyrite formation. Mineralogical Magazine 62A, 151–152.

Benning, L.G., Wilkin, R.T., Konhauser, K.O., 1999. Iron monosulphide stability: experiments with sulphate-reducing bacteria. In: Ármannsson, H. (Ed.), Proceedings of the International Symposium on the Geochemistry of Earth's Surface, 5th, 1999. pp. 429–432, Balkema.

Berner, R.A., 1964. Stability fields of iron minerals in anaerobic marine sediments. Journal of Geology 72, 826–834.

Berner, R.A., 1967. Thermodynamic stability of sedimentary iron sulphides. American Journal of Science 265, 773–785.

Berner, R.A., 1970. Sedimentary pyrite formation. American Journal of Science 268, 1–23.

Boesen, C., Postma, D., 1988. Pyrite formation in anoxic environments of the Baltic Sea. American Journal of Science 288, 575–603.

Bourcier, W.L., Barnes, H.L., 1987. Ore solution chemistry: VII. Stabilities of chloride and bisulfide complexes of zinc to 300°C. Economic Geology 82, 1838–1863.

Cahill, C.L., Benning, L.G., Barnes, H.L., Parise, J., this issue. In-situ, time-resolved X-ray diffraction of iron sulfides during hydrothermal pyrite growth. Chemical Geology.

Calvo, M., Sevillano, E., 1989. Pyrite crystals from Soria and La Rioja provinces, Spain. Mineralogical Magazine 20, 451–456.

Canfield, D.E., Raiswell, R., Bottrell, S., 1992. The reactivity of sedimentary iron minerals towards sulfide. American Journal of Science 292, 659–683.

Canfield, D.E., Raiswell, R., Westrich, J.T., Reaves, C.M., Berner, R.A., 1986. The use of chromium reduction in the analysis of reduced inorganic sulfur in sediments and shales. Chemical Geology 54, 149–155.

Canfield, D.E., Thamdrup, B., Fleischer, S., 1998. Isotope fractionation and sulphur metabolism by pure and enrichment cultures of elemental sulfur-disproportionating bacteria. Limnology and Oceanography 43, 253–264.

Chen, K.Y., Gupta, S.K., 1973. Formation of polysulphides in aqueous solution. Environmental Letters 4, 187–200.

Chen, K.Y., Morris, J.C., 1972. Kinetics of oxidation of aqueous sulfide by O_2. Environmental Science and Technology 6, 529–537.

Davies, C.W., 1962. Ion Association. Butterworth, DC.

Davison, W., 1991. The solubility of iron sulfides in synthetic and natural waters at ambient temperature. Aquatic Sciences 53, 309–329.

Davison, W., Phillips, N., Tabner, B.J., 1999. Soluble iron sulfide in natural waters: reappraisal of their stoichiometry and stability constants. Aquatic Sciences 61, 23–43.

Drobner, E., Huber, H., Wächtershäuser, G., Rose, D., Setter, K.O., 1990. Pyrite formation linked with hydrogen evolution under anaerobic conditions. Nature 346, 742–744.

Furukawa, Y., Barnes, H.L., 1995. Reactions forming pyrite from precipitated amorphous ferrous sulfate. Geochemical Transformations of Sedimentary Sulfur. ACS Symposium Series 612, 194–205.

Giggenbach, W., 1971. Optical spectra of high alkaline sulphide solutions and the second dissociation constant of hydrogen sulphide. Inorganic Chemistry 10, 1333–1338.

Giordano, T.H., Barnes, H.L., 1979. Ore solution chemistry VI. PbS solubility in bisulphide solutions to 300°C. Economic Geology 74, 1637–1646.

Guevremont, J.M., Bebie, J., Elsetinov, A.R., Strongin, D.R., Schoonen, M.A.A., 1998. Reactivity of the (100) plane of pyrite in oxidizing gaseous and aqueous environments: effects of surface imperfections. Environmental Science and Technology 32, 3743–3748.

Haar, L., Gallagher, J.S., Kell, G.S., 1984. NBS/NRC Steam tables. Thermodynamic and transport properties and computer programs for vapour and liquid states of water in SI units. Hemisphere Publishing, Washington.

Herbert, R.B. Jr., Pratt, A.R., Blowes, D.W., Benner, S.G., 1998.

Surface oxidation of iron monosulphide: an X-ray photoelectron spectroscopic study. Mineralogical Magazine 62A, 608–609.

Hurtgen, M.T., Lyons, T.W., Ingal, E.D., Cruse, A.M., 1999. Anomalous enrichments of iron monosulfide in euxinic marine sediments and the role of of H_2S in iron sulfide transformations: examples from Effingham Inlet, Orca Basin, and the Black sea. American Journal of Science 299, 556–588.

Jørgensen, B.B., 1977. The sulfur cycle of a coastal marine sediment. Limnology and Oceanography 22, 814–832.

Kolthoff, I.M., Griffith, F.S., 1938. Studies on ageing and properties of precipitates. XXIII. The postprecipitation of ferrous sulphide with cupric sulphide. Journal of the American Chemical Society 60, 2036–2039.

Krupp, R.E., 1994. Phase relations and phase transformations between low temperature iron sulphides mackinawite, greigite and smythite. European Journal of Mineralogy 6, 389–396.

Landing, W.M., Westerlund, S., 1988. The solution chemistry of iron(II) in Framvaren fjord. Marine Chemistry 23, 329–343.

Langmuir, D., 1997. Aqueous Environmental Chemistry. Prentice-Hall, NJ, 600 pp.

Lasaga, A.C., 1998. Kinetic Theory in the Earth Sciences. Princeton Univ. Press, Princeton, NJ, Chapters 6 and 7.

Lennie, A.R., Redfern, S.A.T., Champness, P.E., Stoddart, C.P., Schofield, P.F., Vaughan, D.J., 1997. Transformation of mackinawite to greigite: an in-situ X-ray powder diffraction and transmission electron microscopy study. American Mineralogist 82, 302–309.

Luther, G.W. III, 1991. Pyrite synthesis via polysulfide compounds. Geochimica Cosmochimica Acta 55, 2839–2849.

Luther, G.W. III, Ferdelman, T.G., 1993. Voltametric characterisation of iron(II) sulfide complexes in laboratory solutions and in marine waters and porewaters. Environmental Science and Technology 27, 1154–1163.

Luther, G.W. III, Rickard, D.T., Theberge, S., Olroyd, A., 1996. Determination of metal (bi)sulfide stability constants of Mn^{2+}, Fe^{2+}, Co^{2+}, Ni^{2+}, Cu^{2+} and Zn^{2+} by voltametric methods. Environmental Science and Technology 30, 671–679.

Lyons, T.W., 1997. Sulfur isotopic trends and pathways of iron sulfide formation in upper Holocene sediments of the anoxic Black sea. Geochimica Cosmochimica Acta 61, 3367–3382.

Mountain, B.W., Seward, T.M., 1998. Stoichiometry and stability of Fe (II) hydrosulphide complexes at 2–100°C. Mineralogical Magazine 62A, 1032–1033.

Mountain, B.W., Seward, T.M., 1999. The hydrosulphide complexes of copper(I): Experimental determination of stoichiometry and stability at 22°C and reassessment of high temperature data. Geochimica Cosmochimica Acta 63, 11–29.

Murowchick, J.B., Barnes, H.L., 1986. Marcasite precipitation from hydrothermal solutions. Geochimica Cosmochimica Acta 50, 2615–2630.

Pratt, A.R., Muir, I.J., Nesbitt, H.W., 1994. X-ray photoelectron and Auger electron spectroscopic studies of pyrrhotite and mechanisms of air oxidation. Geochimica Cosmochimica Acta 58, 827–841.

Renders, P.J., Seward, T.M., 1989. The stability of hydrosulphido- and sulphido complexes of Au(I) and Ag(I) at 25°C. Geochimica Cosmochimica Acta 53, 244–253.

Rickard, D.T., 1969. The chemistry of iron sulphide formation at low temperatures. Stockholm Contributions in Geology 20, 67–95.

Rickard, D.T., 1975. Kinetics and mechanism of pyrite formation at low temperatures. American Journal of Science 275, 636–652.

Rickard, D.T., 1997. Kinetics of pyrite formation by the H_2S oxidation of iron(II) monosulfide in aqueous solutions between 25°C and 125°C: the rate equation. Geochimica Cosmochimica Acta 61, 115–134.

Rickard, D.T., Luther, G.W. III, 1997. Kinetics of pyrite formation by the H_2S oxidation of iron (II) monosulphide in aqueous solutions between 25°C and 125°C: the mechanism. Geochimica Cosmochimica Acta 61, 135–147.

Roberts, W.M.B., Walker, A.L., Buchanan, A.S., 1969. The chemistry of pyrite formation in aqueous solutions and its relation to the depositional environment. Mineralium Deposita 4, 18–29.

Robie, R.A., Hemingway, B.S., Fisher, J.R., 1978. Thermodynamic properties of minerals and related substances at 298.15 K and 1 bar (105 Pascal) pressure and at higher temperatures. Geological Survey Bulletin (United States) 1452.

Schoonen, M.A.A., Barnes, H.L., 1991a. Mechanisms of pyrite and marcasite formation from solution: III. Hydrothermal processes. Geochimica Cosmochimica Acta 55, 3491–3504.

Schoonen, M.A.A., Barnes, H.L., 1991b. Reactions forming pyrite and marcasite from solution: II. Via FeS precursors below 100°C. Geochimica Cosmochimica Acta 55, 1505–1514.

Schoonen, M.A.A., Barnes, H.L., 1991c. Reactions forming pyrite and marcasite from solution: I. Nucleation of FeS_2 below 100°C. Geochimica Cosmochimica Acta 55, 1495–1504.

Suits, N.S., Wilkin, R.T., 1998. Pyrite formation in the water column and sediments of a meromictic lake. Geology 26, 1099–1102.

Suleimenov, O.M., Krupp, R.E., 1994. Solubility of hydrogen sulphide in pure water and in NaCl solutions, from 20°C to 320°C and at saturation pressures. Geochimica Cosmochimica Acta 58, 2433–2444.

Suleimenov, O.M., Seward, T.M., 1997. A spectrophotometric study of hydrogen sulphide ionisation in aqueous solutions to 350°C. Geochimica Cosmochimica Acta 61, 5187–5198.

Sweeney, R.E., Kaplan, I.R., 1973. Pyrite framboid formation: laboratory synthesis and marine sediments. Economic Geology 68, 618–634.

Taylor, P., Rummery, T.E., Owen, D.G., 1979a. On the conversion of mackinawite to greigite. Journal of Inorganic and Nuclear Chemistry 41, 595–596.

Taylor, P., Rummery, T.E., Owen, D.G., 1979b. Reactions of iron monosulfide solids with aqueous hydrogen sulfide up to 160°C. Journal of Inorganic and Nuclear Chemistry 41, 1683–1687.

Tewari, P.H., Wallace, G., Campbell, A.B., 1978. The solubility of iron sulphides and their role in mass transport in Girdler-Sulphide heavy water plants. Report of the Atomic Energy Canada AECL-5960, 1–34.

Vaughan, D.J., Craig, J.R., 1997. Sulfide ore mineral stabilities, morphologies, and intergrowth textures. In: Barnes, H.L. (Ed.), Geochemistry of Hydrothermal Ore Deposits. 3rd edn.pp. 367–434.

Wächtershäuser, G., 1988. Pyrite formation, the first energy source of life: a hypothesis. Systematics Applied Microbiology 10, 207–210.

Wächtershäuser, G., 1993. The cradle chemistry of life: on the origin of natural products in a pyrite-pulled chemoautotrophic origin of life. Pure and Applied Chemistry 65, 1343–1348.

Wagman, D.D., Evans, W.H., Parker, V.B., Halow, I., Bailey, S.M., Schumm, R.H., 1968. Selected values of chemical thermodynamic properties: tables for the first thirty-four elements in the standards order of arrangement. National Bureau of Standards (United States), Technical Note 270–273, 264 pp.

Wei, D., Osseo-Asare, K., 1995. Formation of iron monosulphide: a spectrophotometric study of the reaction between ferrous and sulphide ions in aqueous solutions. Journal of Colloid and Interface Science 174, 273–282.

Wei, D., Osseo-Asare, K., 1996. Particulate pyrite formation by the Fe^{3+}/HS^{-} reaction in aqueous solution: effect of solution composition. Colloids and Surfaces A: Physicochemical and Engineering Aspects 118, 51–61.

Widler, A.M., 1999. Adsorption of gold(I) hydrosulphide complexes by iron sulphides. Unpublished Ph.D. thesis, Swiss Federal Institute of Technology, Zurich, Switzerland.

Wilkin, R.T., Barnes, H.L., 1996. Pyrite formation by reactions of iron monosulfides with dissolved inorganic and organic sulfur species. Geochimica Cosmochimica Acta 60, 4167–4179.

Wilkin, R.T., Barnes, H.L., 1997. Pyrite formation in an anoxic estuarine basin. American Journal of Science 297, 620–650.